Estimating the long-term slip rate of active normal faults: The case of the Paganica Fault (Central Apennines, Italy)

I. Puliti[1,2], S. Pucci[3], F. Villani[3], M. Porreca[2], L. Benedetti[4], G. Robustelli[5], A. Gueli[6], G. Stella[6]

1 Now at Dipartimento InGeo, Università di Chieti- Pescara "G.D'Annunzio", Via dei Vestini 31, 66100 Chieti Scalo, Italy
2 Dipartimento di Fisica e Geologia, Università di Perugia, Piazza dell'Università, 00123 Perugia, Italy
3 Istituto Nazionale di Geofisica e Vulcanologia, Via di Vigna Murata 605, 00143 Rome, Italy
4 Aix-Marseille Université, CNRS-IRD-Collège de France UMR 34 CEREGE, Aix en Provence, France
5 Dipartimento di Biologia, Ecologia e Scienze della Terra, Università` della Calabria, Via P. Bucci, Cubo 15B, 87036 Arcavacata di Rende (CS), Italy
6 PH3DRA labs, Dipartimento di Fisica e Astronomia E. Majorana dell'Università and INFN CT, via Santa Sofia 64, 95123 Catania, Italy

Abstract

The footwall of the surface rupturing Paganica normal fault, the source of the 2009 L'Aquila earthquake (Mw 6.1) in the Central Apennines, was investigated using integrated geological and geomorphological approaches. The aim was to constrain the active tectonics by studying the Raiale River that orthogonally crosscuts the fault trace, where it provides a useful geomorphological marker of long-term fluvial incision and footwall uplift. By morphostratigraphy and paleomagnetic analysis, the Plio–Pleistocene morphotectonic evolution of the area was reconstructed, comprising an ancient continental basin and paleolandforms that predate the footwall incision. Starting from the Late Early Pleistocene–Middle Pleistocene, fluvial dissection was mainly due to marked river downcutting triggered by significant activity of the Paganica fault, which caused progressive base-level lowering. The Raiale River downcutting formed five Middle–Late Pleistocene fluvial terraces that, along with absolute optically stimulated luminescence (OSL) dating, allowed the identification of paleolongitudinal profiles diverging downstream. Terrace dating yielded a minimum incision rate of 0.25 ± 0.02 mm/a, which only partially compensates the footwall uplift and can thus be considered as a minimum value for the Paganica fault throw rate, which could reach up to ~0.45 mm/a. In parallel,

using terrestrial cosmogenic nuclides, a denudation rate of 0.02–0.04 mm/a was measured on the summit of the footwall block. This denudation is in keeping with the drainage incision, suggesting a non-steady state for the fault footwall topography and a dominance of relief growth. Last, the analysis of the modern Raiale River longitudinal profile denoted an ungraded status, with two main knickzones that we interpret as transient forms due to tectonic perturbations, likely triggered by activity of the Paganica fault during the end Early Pleistocene and the Late Pleistocene. Considering the 2009 L'Aquila earthquake coseismic rupture, we observe that the younger transience on the Raiale River longitudinal profile, if it is of tectonic origin, could have been produced only by much larger seismic events (i.e., Mw > 6.5) than those documented in the area by paleoseismological investigations. The results confirmed that in the Apennines, the conditions of dynamic equilibrium are often not met and that the persistence of transient perturbations induced by tectonics should be accounted for.

1. Introduction

In actively deforming areas, landscapes are affected by the interactions between tectonic and climatic changes (Bull, 2011) and undergo erosion and deposition that drive the shape of the topography (Kirby et al., 2012). Overall, drainage systems are susceptible to the external tectonic and climatic factors that may trigger variations on the rivers' concave longitudinal profile in the topographic steady state (i.e., graded or equilibrium profile; Chorley and Kennedy, 1971; Ahnert, 1994; Zhou et al., 2017). Rivers can have small fluctuations over many decades that reflect the short-term changes of boundary conditions, mostly linked to climate (e.g., flow rate and sediment load; Whittaker et al., 2007a; Pazzaglia, 2003; Pérez-Peña et al., 2010). In addition, both local and regional tectonic forces can lead to perturbations on the river graded profile through fault-block dislocations or isostatic adjustments.

In dominant bedrock (detachment-limited) river channels, the lowering of the base level (and/or

uplift) drives the development of a knickpoint/knickzone. This results in a transient state with an ungraded longitudinal profile (Merritts and Vincent, 1989; Whipple and Tucker, 1999; Wobus et al., 2006; Berlin and Anderson, 2007), where the upstream migration of a knickpoint/knickzone represents a regressive wave of incision that progressively restores the equilibrium state through incision or aggradation (Tucker and Whipple, 2002; Harkins et al., 2007; Whittaker et al., 2010).

When tectonic uplift (or subsidence) is balanced by incision (or sedimentation), such quasi-equilibrium conditions (i.e., graded profile) are met. However, this only occurs if the timescale of tectonic changes is larger than the timescale of the channel response. Conversely, if, for example, the rate of footwall uplift due to coseismic surface faulting (hence, the slip per event/recurrence time) exceeds the mean rate of river incision, the ungraded longitudinal profile is preserved in the long term.

Based on this evidence, several studies were published on how the role of tectonics can be independently determined by the theoretical drainage transient response to uplift rate variations (e.g., Whipple and Tucker, 1999, 2002; Snyder et al., 2000; Kirby and Whipple, 2001; Wobus, 2006, Cyr et al., 2010; Pucci et al., 2014; De Gelder et al., 2019). Specifically, rivers counterbalance the footwall uplift of active normal faults and incise valleys (Hancock and Anderson, 2002; Starkel, 2003; Azañón et al., 2005), providing an opportunity to create and preserve relict fluvial landforms through which paleolongitudinal profiles can be reconstructed. The paleolongitudinal profiles represent timelines that are helpful for deducing the evolution of base-level changes and is a valuable tool for estimating the uplift rates (Schumm, 1993; Boogaart and Van Balen, 2000; Hetzel et al., 2002; Watchman and Twidale, 2002; Pérez-Peña et al., 2009).

Geomorphological and Quaternary geological investigations were combined to extract tectonic signals from the incisional history of the Raiale River in the Abruzzi region (Central Italy). The study

area includes the upper reach of the Raiale River that flows on the uplifting footwall and crosses the active Paganica normal fault. This fault is responsible for the major 2009 L'Aquila earthquake (Mw 6.1), which produced surface coseismic faulting and caused considerable damage and fatalities (Emergeo Working Group, 2009; Pondrelli et al., 2010; Scognamiglio et al., 2010; Herrmann et al., 2011).

This study focused on two elements: (1) reconstruction of the Quaternary evolution of the area, supported by chronological constraints of the continental deposits, with emphasis on the fluvial history, to unravel depositional and erosional processes that occurred at the footwall of the Paganica fault as a response to local tectonic forcing and (2) estimation of an independent long-term throw rate of the Paganica fault for comparison with near-fault measurements made with other techniques (Galli et al., 2010; Boncio et al., 2010; Roberts et al., 2010; Cinti et al., 2011, Moro et al., 2013; Villani et al., 2017; Civico et al., 2017).

To achieve these, a combination of new field surveys of Quaternary continental and late Pleistocene–Holocene fluvial terrace deposits with paleomagnetic and optically stimulated luminescence (OSL) dating techniques was performed. The morphostructural reconstruction of depositional bodies and erosional landforms was performed by integrating different datasets from aerial photos and high-resolution topography (LiDAR-derived digital elevation model (DEM)) interpretations.

The long-term activity (i.e., throw rate) of the Paganica fault was obtained by investigating the adjustment of the Raiale River longitudinal profile to ongoing footwall uplift by channel incision. Specifically, in the hypothesis that the Raiale River tends to a topographic steady state (i.e., equilibrium) through a transient response to tectonic perturbation, the channel incision rate approaches the rate of tectonic uplift. In agreement with the theoretical models of normal faults (Lavé and Avouac, 2001), the maximum footwall uplift occurs at the surface trace of the Paganica fault, as

shown by the surface rupture patterns from InSAR data after the 2009 earthquake (Atzori et al., 2009). Thus, near the fault, in correspondence with the lower drainage reaches (i.e., the main stem), we also expect the most significant channel incision rates. Particular attention was given to mapping and dating the fluvial terrace flights preserved along the Raiale upper reach as evidence of paleotalweg levels and progressive channel downcutting to acquire a reliable river incision rate.

The denudation rate was measured at the summit of the drainage incising the footwall block using cosmogenic exposure dating to evaluate the landscape sensitivity to the disturbing tectonic forces. Last, the results were considered alongside published data on the long-term and 2009 L'Aquila earthquake activity of the Paganica fault, which are produced through independent methodologies. Moreover, the effect of fault activity on the relief dynamics is discussed in the following sections.

2. Seismotectonic and geological setting

The study area is located in the axial sector of the Central Apennines range, a Neogene NE-verging fold-and-thrust belt developed along the Adriatic microplate's margin and affected by multiphased contractional extensional deformation (Carminati and Doglioni, 2012). Following the subaerial summit exposure that occurred during the Messinian–Early Pliocene more than 5 Ma ago (Bosi et al., 2003; Centamore et al., 2006), a post-orogenic Pliocene–Quaternary extension dissected the compressional edifice, mainly by NW-striking and SW-dipping normal faults. These normal faults are arranged in systems, generally not exceeding 30 km in length (Galadini and Galli, 2000; Boncio et al., 2004a, and 2004b; Roberts and Michetti, 2004), showing evidence of late Pleistocene–Holocene surface-rupturing earthquakes (Galli et al., 2008; Benedetti et al., 2013). The present-day active NE-trending extension predominantly occurs along the axis of the chain, as displayed by upper crustal instrumental seismicity (Chiarabba et al., 2005; Bagh et al., 2007; Pondrelli et al., 2010; Rovida et al., 2016) and geodetic horizontal velocities of ~1–3 mm/a (Hunstad, 2003; D'Agostino et

al., 2011; Devoti et al., 2011; Carafa and Bird, 2016). Along the Apennines chain, the active normal fault systems controlled the evolution of the intermontane basins developed in their hanging wall and infilled with Plio–Quaternary continental deposits (Cavinato and De Celles, 1999). These basins represent a geological archive of past tectonic events and climatic fluctuations, which occurred in a setting characterized by a large-scale uplift since the Early–Middle Pleistocene (D'Agostino et al., 2001).

2.1. Geological setting of the Plio–Quaternary Middle Aterno basin

The Middle Aterno Valley (MAV) is one of the main intermontane tectonic basins in the Central Apennines. It is an initially isolated Plio–Quaternary continental depression, which became fluvially integrated into the Aterno River system and the Adriatic coast during the late Early–Middle Pleistocene (Geurts et al., 2020). The MAV is controlled by the long-term activity of a composite network of right-stepping normal fault segments generally trending NW and dipping to the SW. This fault system is known as the Paganica-San Demetrio fault system (PSDFS) and it is mainly composed of two major faults that define this active fault array, namely, the Paganica (PAG) to the north–west, and the San Giovanni (SAG) faults to the south–east (Galli et al., 2010; Lavecchia et al., 2012; Civico et al., 2015; Giaccio et al., 2012; Pucci et al., 2019).

This region has a strong seismogenic potential, attested by instrumental earthquakes (Pace et al. 2006; Pondrelli et al., 2010; Scognamiglio et al., 2010; Peruzza et al. 2011; Herrmann et al., 2011) and historical reports (Tertulliani et al., 2009). The PAG ruptured during the 2009 Mw 6.1 earthquake (Atzori et al., 2009; Pondrelli et al., 2009; Papanikoloaou et al., 2010; Valoroso et al., 2013), causing primary surface faulting with coseismic throws up to ~15 cm, consistent with the SW-dipping geometry and kinematics of the main fault plane (Emergeo Working Group, 2009; Boncio et al., 2010) (Fig. 1). Coseismic deformation was also observed in the far-field through the Envisat and

142 COSMO-SkyMed DInSAR interferograms that recorded a maximum footwall uplift of 5–10 cm
143 (Atzori et al., 2009). Paleoseismic records also point out recurrent Holocene ruptures along the
144 PSDFS with an average recurrence time of ~300–500 years and 1000–2000 years for 2009-like and
145 Mw > 6.5 events, respectively (Galli et al., 2011; Cinti et al., 2011; Moro et al., 2013; Blumetti et al.,
146 2017). The paleo-faulting events produced throws larger (i.e., ~50 cm) than those occurred in 2009
147 (Cinti et al., 2011; Moro et al., 2013).

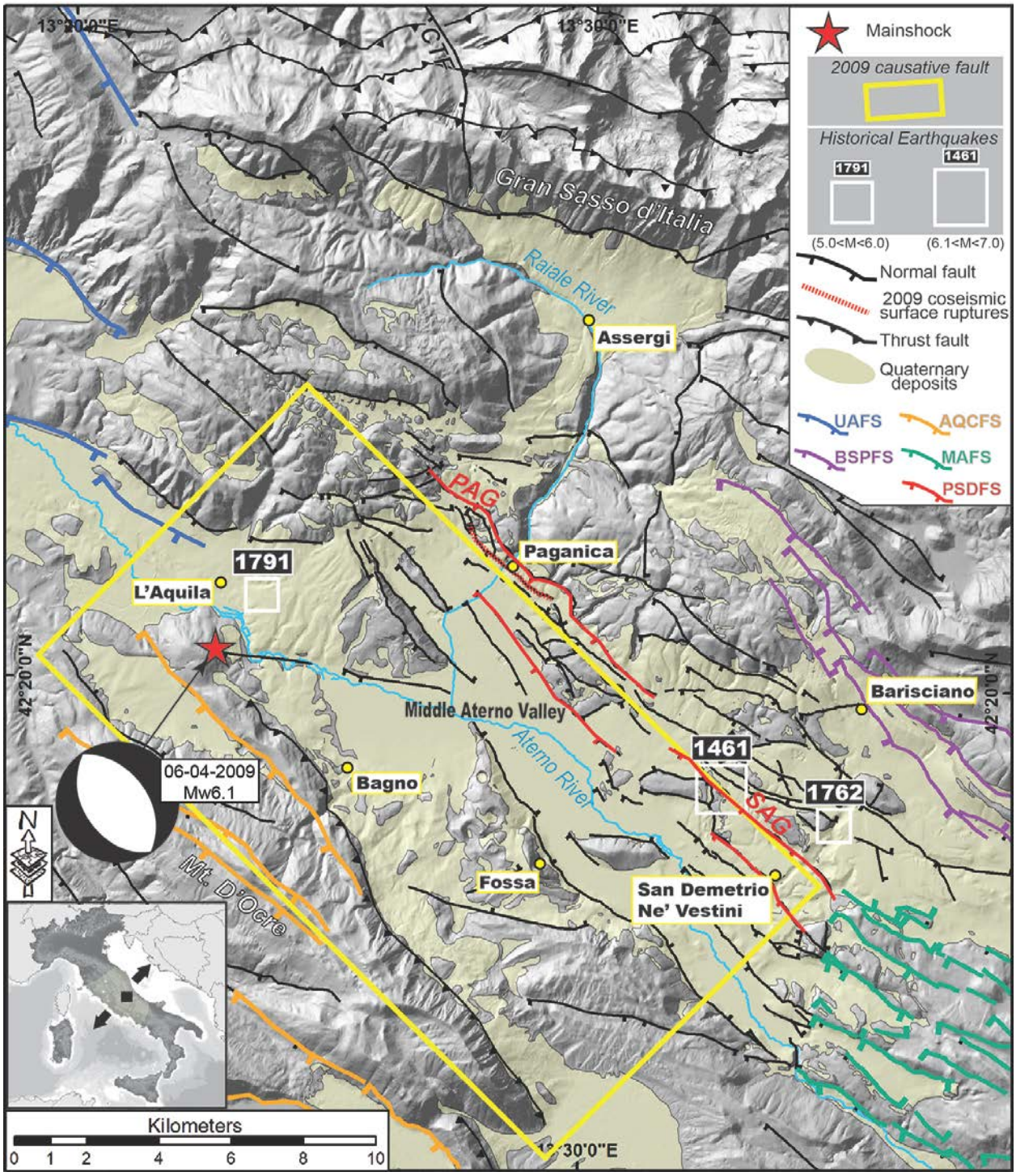

148

149 **Figure 1.** Location map of the 2009 L'Aquila mainshock (Scognamiglio et al., 2010; Herrmann et al., 2011). Focal
150 mechanisms of the mainshock, historical seismicity (Mw > 5.0, open squares; https://emidius.mi.ingv.it/CPTI15-
151 DBMI15/), and main surrounding active fault systems are shown (acronyms as follows: UAFS, Upper Aterno Fault
152 System; PSDFS, Paganica-San Demetrio fault system, of which PAG and SAG are the main fault segments; BSPFS,
153 Barisciano-San Pio fault system; MAFS, Middle Aterno fault system (modified after Galadini and Galli, 2000; Civico et
154 al., 2015; Pucci et al., 2015). According to several investigators, the yellow box is the approximate projection to the

surface of the ~19-km-long 2009 mainshock causative fault (Vannoli et al., 2012 and Chiaraluce, 2012). DEM from 10-m resolution TIN-Italy (Tarquini et al., 2012).

The tectonic-sedimentary evolution of the MAV basin results from the interplay of early E–W- and N–S-trending conjugate faults and the main NW–SE-trending normal fault systems (Blumetti et al., 2013; Pucci et al., 2019) (Fig. 2). This interplay prompted a compound continental deposit infilling (GE.MI.NA., 1963; Bertini and Bosi, 1993; Messina et al., 2001; Bosi et al., 2003; Aneglino et al., 2010; Tallini et al., 2012; Giaccio et al., 2012; Spadi et al., 2016; Nocentini et al., 2018; Pucci et al., 2019), with isolated depocenters thickening up to 500–600 m (Cesi et al., 2010; Balasco et al., 2011; Improta et al., 2012; Villani et al., 2015 and 2017; Santo et al., 2014; Pucci et al., 2016; Porreca et al., 2016; Civico et al., 2017).

Based on Giaccio et al. (2012) and Pucci et al. (2019) studies, the conjugated E–W and N–S-trending faults during the Late Pliocene–Early Pleistocene mostly controlled the oldest sedimentary traps, characterized by syntectonic deposition, thickness variability, and hiatuses. Most of the old infill is composed of widespread mass-wasting deposits of typical proximal facies, mainly composed of slope-breccias and rock-slide deposits (Valle Valiano Breccia -VVB-, Megabrecce -MEB-, Cesarano Breccia -CEB-, L'Aquila Breccia -LAB-) and sparse alluvial fan conglomerates (Valle Valiano Conglomerates Fm. -VVC) (Pucci et al., 2019). During the Late Pliocene–Early Pleistocene, extensive lacustrine and SE-flowing fan delta deposition (San Nicandro Fm. -SNL- and Vall'Orsa Conglomerates Fm. -VOC, respectively) occurred. Spadi et al. (2016) reported evidence of the late Piacenzian age fossils, witnessing possible older inception of the SNL lacustrine environment. Later, the NW-trending fault set became predominant at the end of the Early Pleistocene. Consequently, a prominent ~19-km-long fault system (PSDFS) dissected the proto-MAV, bounding the 3–6-km-wide Paganica-San Demetrio basin. This kinematic change likely promoted a drastic reorganization of the fluvial system, inducing a prevailing SW-flowing alluvial fan deposition (Valle Inferno Fm. -VIC,

San Mauro -SMA-, ALP and ALH Fms.; Bagnaia et al.,1992; Giaccio et al., 2012; Nocentini et al., 2018; Pucci et al., 2019).

In the northern sector of the Paganica-San Demetrio basin, the PAG, along with its set of subparallel normal fault splays, acted as the leading strand in accruing most of the long-term displacement of the PSDFS (~650 m of cumulative net throw; Pucci et al., 2016; Villani et al., 2017). The long-term subsidence of the PAG hanging wall triggered the aggradation of the >80-m-thick alluvial fans of the Raiale River, ranging in age from the Middle Pleistocene to the Holocene (Galli et al., 2010; Giaccio et al., 2012) and showing evident Middle Pleistocene syntectonic growth as suggested by high-resolution seismic data (Villani et al., 2017). In addition, the uplift of the PAG footwall block caused the deep gorge along the Raiale River's upper reach, wind gaps, elevated erosional surfaces, and beheaded toes of Pliocene–Early Pleistocene breccia bodies at the Camarda basin (Pucci et al., 2019) (Fig. 2). Paleoseismological, geophysical, and morphotectonic studies on the PAG (Galli et al., 2010; Boncio et al., 2010; Roberts et al., 2010; Cinti et al., 2011, Moro et al., 2013; Macrì et al., 2016; Villani et al., 2017; Civico et al., 2017) suggested long-term throw rates of 0.1–0.4 mm/a for the last 1–2 Ma, 0.5 mm/a for the last 450 ka, and 0.1–0.3 mm/a for the last 30 ka.

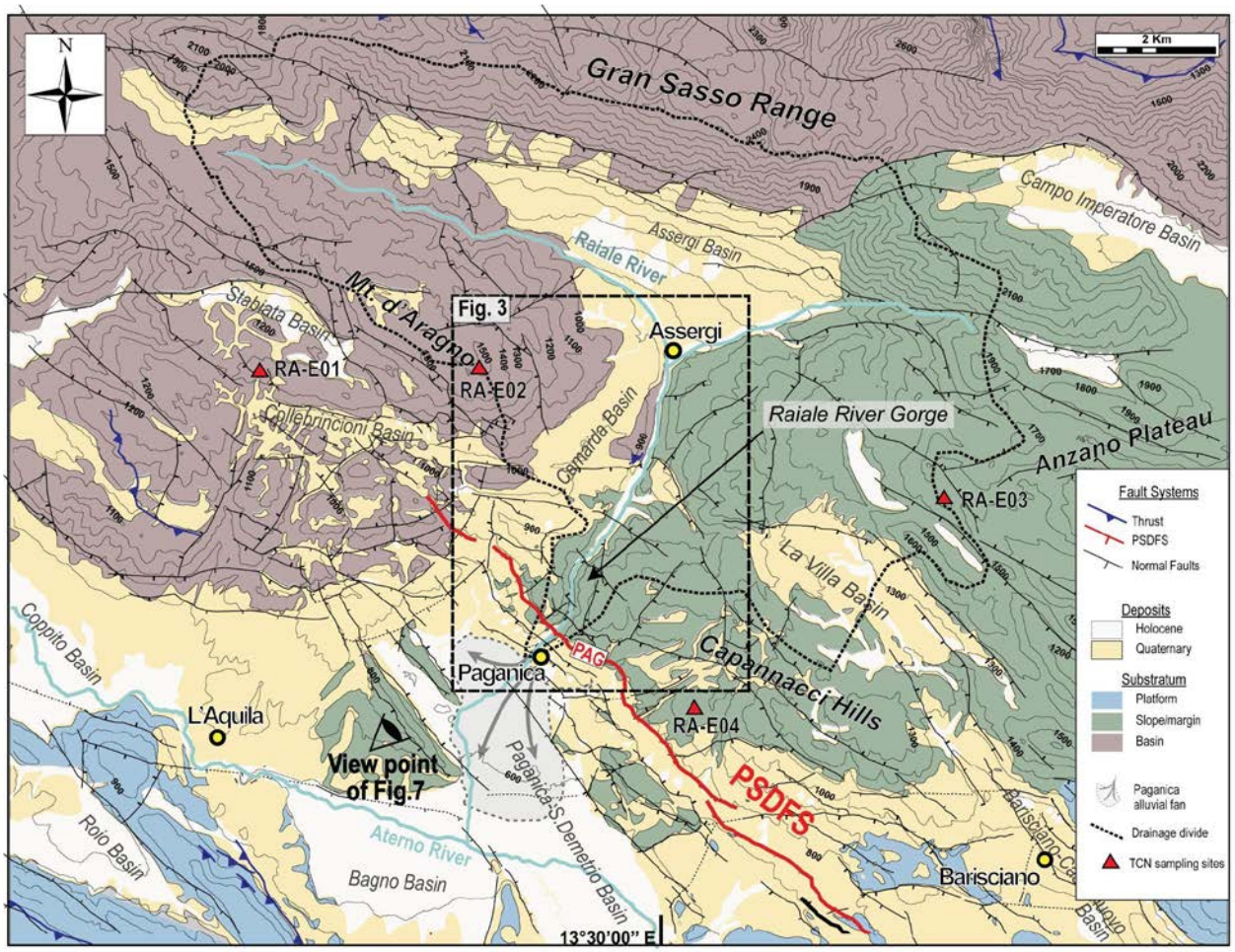

Figure 2. Structural map of the study area (modified after Pucci et al., 2019). The NW-trending and the conjugated W- and N-trending normal faults are in black. The PSDFS is shown with a thick red line. The PAG segment is labeled. Thrust faults are in blue. The three main substratum paleogeographic domains are indicated with different colors: Umbria-Marche basinal domain and Latium-Abruzzi platform and margin domains (Centamore et al., 2006). The Holocene and Plio–Pleistocene continental deposit locations are outlined, together with the major catchment divide of the Paganica alluvial fan and the Raiale River. The red triangles indicate the sites of sampling for Terrestrial Cosmogenic Nuclides dating.

3. Materials and methods

To depict the Quaternary evolution of the landscape at the footwall block of the active Paganica fault and to evaluate how its activity contributed to this evolution, a combination of field surveys, morphometric analysis, and Quaternary deposit and landform dating was conducted.

3.1 Quaternary geological map

To define the Quaternary evolution of the Paganica fault footwall, the tectonic and stratigraphic framework was reconstructed, from which geomorphic and depositional markers of long-term incision, denudation, and fault displacement can be deciphered. First, a detailed mapping of tectonic structures and continental deposits was performed through field surveys, aerial photo interpretation from 1:33,000 scale stereo pairs (Istituto Geografico Militare - Gruppo Aereo Italiano flights, 1954–1955), and raster imagery (Orthophoto Regione Abruzzo 2007). The applied morphostratigraphic analysis benefited from a DEM (5.0 m/pixel size, from topographic data) and a high-resolution (1.0 m/pixel size) digital surface model (DSM). The latter comes from processing airborne lidar data acquired by the Civil Protection of Friuli Venezia Giulia Region a few days after the 2009 L'Aquila earthquake (using an Optech Airborne Laser Terrain Mapper System; Civico et al., 2015).

The resulting map integrates and updates the Quaternary geological mapping of Pucci et al. (2015 and 2019), which covers a limited portion of the Paganica fault footwall block. In particular, this study focuses on the geometry, extent, and arrangement of the poorly known continental sequence infilling the Camarda basin and Quaternary faults' cross-cut relationships with the Raiale River valley inset deposits. The stratigraphy of the pre Plio–Quaternary bedrock follows the subdivision proposed by the Geological Map of Italy, scale 1:50,000 (sheets 359 L'Aquila and 349 Gran Sasso; ISPRA, 2009), without internal subdivision. Quaternary stratigraphy is based on the scheme proposed by Pucci et al. (2019), integrated with original geological field data.

3.2 Geomorphological analysis

The study was conducted with morphometric analysis to individuate detailed fluvial and alluvial landforms useful to constrain paleobase levels.

First, we extracted from the 5-m DEM of the longitudinal topographic profile of the Raiale River and investigated its shape and channel steepness index (K_{sn}) using the dedicated MATLAB-based

230 software for topography analysis (TopoToolBox; Schwanghart and Scherler, 2014) and Stream
231 Profiler (a free routine for MATLAB in ArcGIS, from Wobus et al., 2006). K_{sn} is a geomorphic index
232 estimated by normalizing the drainage area of a given reach and using a reference concavity that
233 corresponds to the regional concavity observed in reaches unperturbed by tectonic signals (Wobus et
234 al., 2006). This analysis allowed the detailed reconstruction of the present-day Raiale River talweg
235 longitudinal profile, its features (e.g., knickpoint/knickzone), and the reconstruction of the profiles
236 prior to knickpoint propagation.

237 Afterward, fluvial terrace surfaces were identified along with their inner (i.e., the junction between
238 the terrace tread and the valley slope) and outer edges (i.e., the junction between the terrace tread and
239 the talweg riser), remnants of alluvial fans, paleosurfaces, paleovalleys, and wind gaps, stream
240 entrenchments and gullies, and tectonic escarpments through the high-resolution DSM and its
241 derivative slope and hillshade maps (through ArcGIS software tools).

242 Particular attention was paid to identifying and correlating fluvial terraces that flank the lower section
243 of the Raiale River valley as remnants of the former talweg of the main stem. Afterward, the mapped
244 fluvial terraces were checked in the field to assess their strath- or fill-nature. Since colluvial and slope
245 deposits may affect the measurements of risers, by burying the inner edges of the terraces, we
246 correlated the outer edge based on surface morphology, lateral continuity, and altimetric distribution
247 to define different orders of alluvial surfaces. Elevations of river terrace features have been projected
248 onto a common baseline given by the smoothed longitudinal profile of the Raiale River. Profile
249 smoothing was done using spatial analyst tools in ArcGIS to highlight only the main long-wavelength
250 features in the profile, minimizing some possible unwanted features (i.e., small manufactured dams).
251 The elevation values assigned to each terrace feature represent the key elevation (i.e., the dominant
252 elevation) of the outer edge (i.e., the intersection between the terrace tread and the talweg riser). After

253 the projection of the terrace flight above the baseline, the correlation of the different orders of terraces
254 has been obtained through the construction of the linear trendline. Aware of the simplifying
255 assumption of a nearly constant-slope geomorphic marker, a linear correlation was used between
256 terrace remnants in the middle–lower course of the Raiale Valley. In fact, our data indicate that this
257 is a good approximation that well reproduces the general trend of the terrace. Only correlations with
258 coefficient values $R2 > 0.8$ were retained.

259 **3.3 Incision and denudation rate estimate**

260 In continental extensional settings, erosional or depositional processes at fault footwall and hanging
261 wall blocks result from the interplay between slip rates and large-scale regional uplift or subsidence
262 rates (Bull, 2008). Since, in the Central Apennines, the normal fault footwall uplift rate is
263 superimposed on regional uplift (D'Agostino et al., 2001), the footwall area is dominated by erosional
264 processes. Here, along with gravitational phenomena (Hippolyte et al., 2006), channel incision,
265 hillslope, and summit denudation work together in landscape modeling.

266 To unravel the contribution of the PaF activity in landscape building and to reconstruct its long-term
267 throw rate, denudation and incision rates at the footwall block were estimated and compared.

268 The incision rate estimate of the Raiale River is based on the elevation and age of the lowest
269 paleolongitudinal profile. This was directly dated by sampling its terraced deposit using the OSL
270 dating methodology (Section 3.3). The ages of other terraces were inferred by correlation with the
271 oxygen isotope stages (OISs) curve of Lisiecki and Raymo (2005) in the hypothesis of quasiconstant
272 incision rate through time. We tested such a correlation of the age of the fluvial terrace with the OIS
273 because of their climatic origin, as suggested by paleoclimatic studies of Giraudi et al. (2005) on the
274 nearby Gran Sasso Massif and by geomorphological studies in the Apennines (Coltorti et al., 1991,
275 Wegmann and Pazzaglia, 2009, Nesci et al., 2012). Specifically, terrace deposition mainly occurs in

correspondence with glacials (i.e., cold periods), when alluvial sedimentation increases due to enhanced degradation processes, whereas, during interglacials (i.e., temperate-warm periods), widespread vegetation prevents the significant transport of sediment load, and streams cut down into the alluvial sediments.

The denudation rate was determined at the summits (i.e., watershed and interfluves) of the Raiale River drainage basin from the in situ produced cosmogenic nuclide ^{36}Cl measurements (Dunai, 2010, Ryb et al. 2014, Godard et al. 2016). The in situ produced ^{36}Cl cosmogenic nuclide (half-life 301 ka) is the product of the interaction between cosmic particles and mainly Ca atoms in limestones (Schimmelpfennig et al. 2011). Four sites were sampled on the carbonate paleosurface at the interfluve edges of the Raiale basin in the vicinity of the PAG fault trace. Such smoothed summits represent remnants of the oldest land surfaces (possibly related to the oldest Apennines subaerial exposure), which are less affected by fluvial headward erosion.

First, samples were crushed and sieved. Only the fraction of rock whose diameter was between 250 µm and 1 mm was used in the chemical preparation. Afterward, the rock samples were treated, and ^{36}Cl precipitation was obtained. Finally, we measured the concentrations of these precipitates by accelerator mass spectrometry (AMS) at the French CEREGE institute in Aix en Provence, and the denudation rates were obtained according to the procedure by Schimmelpfennig et al. (2009). The measured ^{36}Cl concentrations were determined in the AMS and normalized to a standard prepared by K. Nishiizumi (KNSTD1600, with a nominal $^{36}Cl/^{35}Cl$ value of $2.11 \pm 0.06 \times 10–12$; Sharma et al. 1990; Fifield et al., 1990). The analytical uncertainties include counting statistics, machine stability, and blank correction. Last, the incision rates of the Raiale River valley and the denudation of the nearby summit were compared to provide a picture of the PAG footwall block landscape evolution.

3.4 Dating methods

To constrain the age of the Quaternary deposits and better understand their stratigraphic relations based on outcrop conditions and preservation of rock material, six sites suitable for dating with OSL and paleomagnetic analysis were chosen. In those sites, the following dating methods to cover different age ranges were applied: (1) paleomagnetic analysis on 62 samples collected over five sites and (2) OSL on one sample.

Paleomagnetic analysis was performed at the Paleomagnetism Laboratory of the Istituto Nazionale di Geofisica e Vulcanologia (INGV) in Rome to infer the age of the old breccia deposits. The measure of the natural remaining magnetization of the rock sample has been driven with a cryogenic magnetometer 2G based on the superconductivity of helium liquid. Each set of samples was organized into two subsets to obtain accurate measures, and two different methods demagnetized them: thermal demagnetization and alternate field according to methods described by Messina et al. (2001) and Saroli et al. (2015). Five sites were chosen based on morphostratigraphic relationships, and samples were drilled in the field using a gasoline-powered drill, one for each breccia deposit (Fig. 3). The target breccia or conglomerate deposits are characterized by a significant percentage of the fine-grained and cemented matrix as it is the only component of these continental deposits able to be magnetized during sedimentation. The main magnetic components for each site were analyzed through the Remasoft software and the paleomagnetic mean vector representing the magnetization was calculated (i.e., magnetic polarity; Chadima et al., 2006). Subsequently, the magnetic polarity of the sampled sequence was ascribed to the time scale through the stratigraphic relationships of the sampled deposits.

OSL techniques were performed to date the fluvial deposits composed of quartzitic fine layers. Standard sampling techniques were utilized for poorly lithified materials, sampling by hammering a 15-cm-long aluminum tube into a silty–sandy layer at 0.7 m from the vertical outcrop cut and 1.0 m

322 from the surface of the tread and by collecting ~1.0 kg of sediment for dose rate measurement. Sample
323 preparation and OSL (Aitken, 1985) were conducted at the PH3DRA laboratory of the Department
324 of Physics and Astronomy “E. Majorana”, University of Catania (Italy) Equivalent dose (ED) rates
325 were obtained from the extracted coarse-grained quartz fraction through single-aliquot regenerative-
326 dose protocol (Murray and Wintle, 2003) using a Risø TL-DA-15 reader equipped with an
327 EMI9235QA photomultiplier (Bøtter-Jensen et al., 2000). The feldspar contamination was checked
328 using the IR stimulation (Choi et al., 2009). Only the aliquots that passed the recycling (Roberts,
329 2006) and recovery (Murray and Wintle, 2003) tests were considered for ED evaluation. All
330 procedures were performed in dim red light. Dose rate measurements were obtained from high-
331 resolution gamma spectrometry measurements (HPGe). Ages were derived from the ratio between
332 ED and dose rate.

333 **4. Results**

334 The Raiale River crosses the PAG fault trace orthogonally, and its set of subparallel splays and
335 hydrologically connects the Assergi (1000–900 m a.s.l.) and the Paganica basins (~600 m a.s.l.)
336 flowing through the Camarda (800–700 m a.s.l.) basins on its footwall (Fig. 2). Owing to the Camarda
337 area location respect to the main PAG fault trace, it offered valuable hints on the Quaternary
338 sedimentation and drainage evolution to constrain the fault activity.

339 **4.1 Geology and stratigraphy**

340 A new 1:10,000-scale geological map was produced (Fig. 3), yielding details on the distribution of
341 the Quaternary continental deposits along the Raiale River. Along with three geological sections (Fig.
342 4), it illustrates the relationship of these deposits with the main tectonic structures.

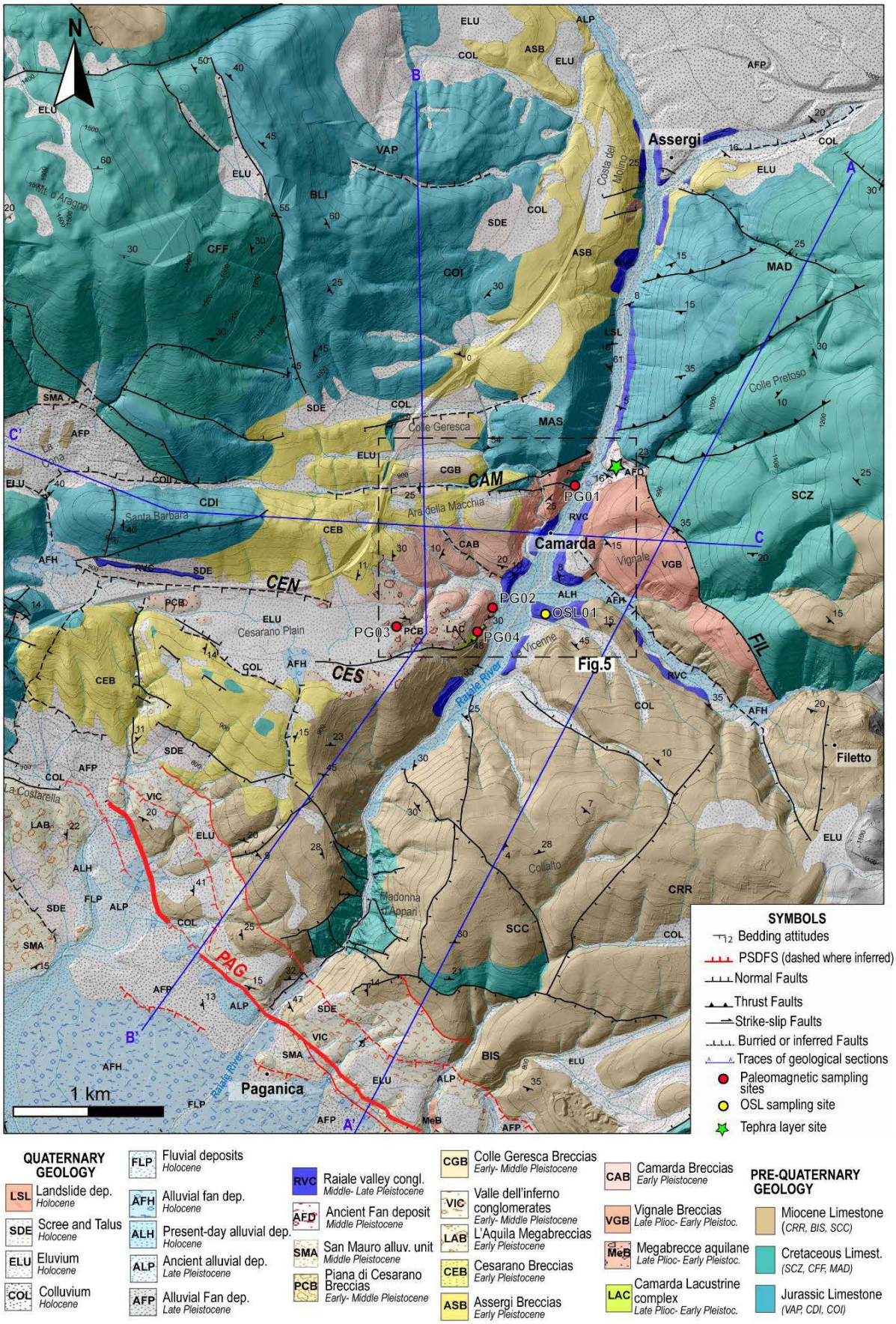
N
Assergi
Camarda
Filetto
Paganica
Colle Geresca
Colle Pretoso
Costa del Molino
Vignale
Cesarano Plain
Santa Barbara
Aragno
Collalto
Madonna d'Appari
La Costarella
Vicenne
Raiale River
Mt. d'Aragno
PG01
PG02
PG03
PG04
OSL01
Fig.5
A
A'
B
B'
C
C'
CAM
CEN
CES
FIL
PAG
1 km
SYMBOLS
Bedding attitudes
PSDFS (dashed where inferred)
Normal Faults
Thrust Faults
Strike-slip Faults
Burried or inferred Faults
Traces of geological sections
Paleomagnetic sampling sites
OSL sampling site
Tephra layer site
QUATERNARY GEOLOGY
LSL Landslide dep. Holocene
SDE Scree and Talus Holocene
ELU Eluvium Holocene
COL Colluvium Holocene
FLP Fluvial deposits Holocene
AFH Alluvial fan dep. Holocene
ALH Present-day alluvial dep. Holocene
ALP Ancient alluvial dep. Late Pleistocene
AFP Alluvial Fan dep. Late Pleistocene
RVC Raiale valley congl. Middle- Late Pleistocene
AFD Ancient Fan deposit Middle Pleistocene
SMA San Mauro alluv. unit Middle Pleistocene
PCB Piana di Cesarano Breccias Early- Middle Pleistocene
CGB Colle Geresca Breccias Early- Middle Pleistocene
VIC Valle dell'inferno conglomerates Early- Middle Pleistocene
LAB L'Aquila Megabreccias Early Pleistocene
CEB Cesarano Breccias Early Pleistocene
ASB Assergi Breccias Early Pleistocene
CAB Camarda Breccias Early Pleistocene
VGB Vignale Breccias Late Plioc- Early Pleistoc.
MeB Megabrecce aquilane Late Plioc- Early Pleistoc.
LAC Camarda Lacustrine complex Late Plioc- Early Pleistoc.
PRE-QUATERNARY GEOLOGY
Miocene Limestone (CRR, BIS, SCC)
Cretaceous Limest. (SCZ, CFF, MAD)
Jurassic Limestone (VAP, CDI, COI)

Figure 3. Detailed Quaternary geological map of the Raiale River basin (Fig. 2). Substratum from Carta Geologica d'Italia, scale 1:50,000 Sheet 359 L'Aquila, ISPRA: Jurassic limestones are Calcare Massiccio (MAS), Corniola (COI), Verde Ammonitico (VAP), and Calcari Diasprigni Detritici formations; Cretaceous limestones are Maiolica (MAD), Calcareniti e Calciruditi a Fucoidi (CFF), and Scaglia Detritica (SCZ) formations; and Paleogene–Neogene limestones are Scaglia Cinerea (SCC), Bisciaro (BIS), and Marne con Cerrogna (CRR) formations. 1-m resolution shaded DTM from Lidar (Civico et al., 2015). Blue traces indicate geological cross sections of Fig. 4. Red circles are the sampling sites of paleomagnetic dating, and yellow circles indicate the OSL sampling site (Section 3.3.).

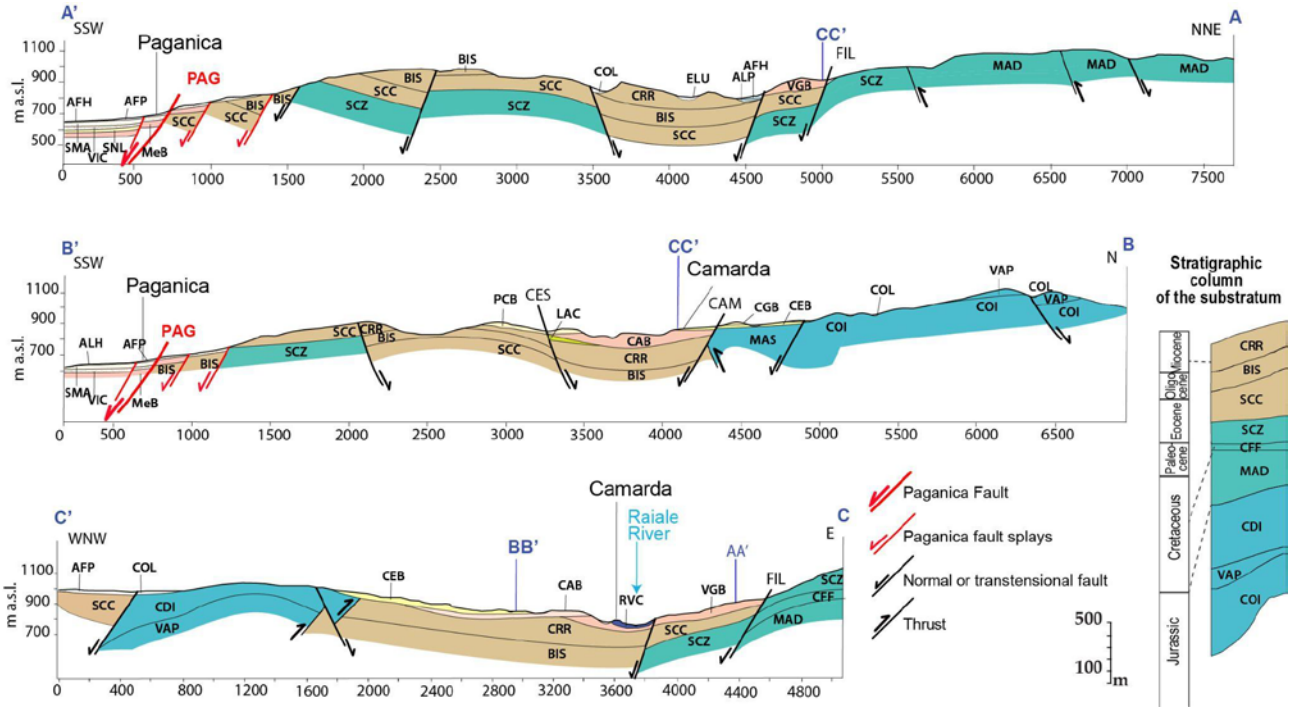

Figure 4. Geological cross sections orthogonal to the PAG fault splays (in red) and the main compressional structures (AA' and BB') and parallel to the Camarda basin axis (CC'). See Fig. 3 for the location of the cross section traces. Plio–Quaternary deposits are labeled (COL, AFP, ALF, VIC, SMA, LAC, PCB, CAB, CEB, CGB, VGB, and RVC) and described both in Fig. 3 and in the main text.

The bedrock of the study area is characterized by Jurassic basinal formations, mainly located northwest of the Raiale River, that override the Cretaceous–Tertiary ones of the slope/margin domain through two high-angle, SW–NE-trending faults, with transpressive and kinematics, outcropping close to the Camarda village (Fig. 3). In addition to that, in the area, extensional structures dominate. Some record preQuaternary displacement of ~200–300 m, with no evident morphological offset, whereas others, such as the CAM fault, are well-expressed in the morphology and control the

362 Quaternary continental deposition. In particular, as part of the two main normal fault systems, the
363 total fault displacements are accommodated by the E–W-trending Cesarano (CES; ~80 m) and
364 Assergi (ASF; ~1000 m from Pizzi et al. 2002) faults; the NW–SE-trending Filetto (FIL; ~230 m)
365 and Paganica faults (PAG; ~650 m, from Villani et al., 2017) (Figs. 3 and 4). These faults appear to
366 control the northern boundary of the main continental basins of the area, which are, from NE to SW,
367 the Assergi, the Camarda, and the Paganica basins.

368 **4.1.1 Continental deposits**

369 The Paganica basin is characterized by the aggradation of the large Middle Pleistocene–
370 Holocene alluvial fan at the Raiale River outlet. Along its eastern edge, it is characterized by a narrow
371 staircase of Early–Middle Pleistocene to Late Pleistocene alluvial terraces (units ALP, SMA, and VIC
372 Fms., Fig. 3), covering a matrix-supported Plio–Pleistocene breccia (MEB Fm., Fig. 3). These alluvial
373 terraces are displaced by the activity of the PAG splays, which also dissect alluvial fan apexes.

374 The Assergi basin is mantled by coalescent Middle–Late Pleistocene alluvial fan deposits (AFD in
375 Fig. 3) comprising planar to cross-stratified silt, sand, and conglomerates, southwestern dipping,
376 derived from the dismantling of the Gran Sasso southern slope at the ASF footwall.

377 The Camarda area presents continental deposits exposed by the Raiale River incision and is located
378 in an open syncline structure (cross section BB', Fig. 4). The continental sequence comprises five
379 confined bodies of clayey silt and breccias represented by the lacustrine deposit (LAC Fm.), the
380 slope/cataclastic Vignale Breccia Formation (VGB Fm.), the exotic clast-bearing Camarda Breccia
381 Formation (CAB Fm.), and the proximal alluvial Cesarano (CEB Fm.) and Piana di Cesarano (PCB
382 Fm.) Breccia Formations (Fig. 5) (see A1 in Supplementary Materials). This depositional sequence
383 results from low energy to proximal, high-energy depositional environment unrelated to the present-
384 day Raiale fluvial system. From the stratigraphic relationship among LAC, CAB, and VGB as well

as the large back tilt (>40°) of the lacustrine layers, it is inferred that the Camarda basin is a syntectonic depression controlled by the E- and NNW-trending CES, CEN, CAM, and FIL faults (Fig. 3 and 5c).

The paleomagnetic sampling has been conducted on the LAC, CAB, VGB, and PCB Formations to support the reconstruction of the Camarda basin stratigraphy (Fig. 5; see Tab. A2 and Fig. S2 in Supplementary Material A2 for details). In particular, the LAC and VGB Formations (samples PG04 and PG01, respectively) yield a normal magnetic polarity (Fig. 5a). The CAB Fm. (deposited after the LAC) shows a reverse magnetic polarity (PG02 sample in Figs. 5a and 5b). Finally, the sequence is closed by the PGB Fm. (Figs. 5b and c), which records a normal magnetic polarity (PG03).

The normal polarity of the lower members (LAC and VGB Fms.) might indicate a Pliocene age of deposition (Gauss normal polarity chron), in agreement with the micropaleontological record of the San Nicandro lacustrine deposits of the Paganica-San Demetrio basin (Spadi et al., 2016). The magnetic reversal observed for the CAB Fm. might suggest an Early Pleistocene age (Matuyama reversed polarity chron), whereas the normal polarity recorded in the upper part of the sequence (PCB Fm.) suggests a Middle Pleistocene age (Brunhes normal magnetic chron). Magnetic polarities and stratigraphic relationships chronologically constrain the Camarda basin to the Pliocene–Early Pleistocene. We do not rule out a possible coeval Late Pliocene onset of the lacustrine deposition (LAC Fm.) with that of the MAV basin (SNL Fm.) (Giaccio et al., 2012; Spadi et al., 2016; Pucci et al., 2019).

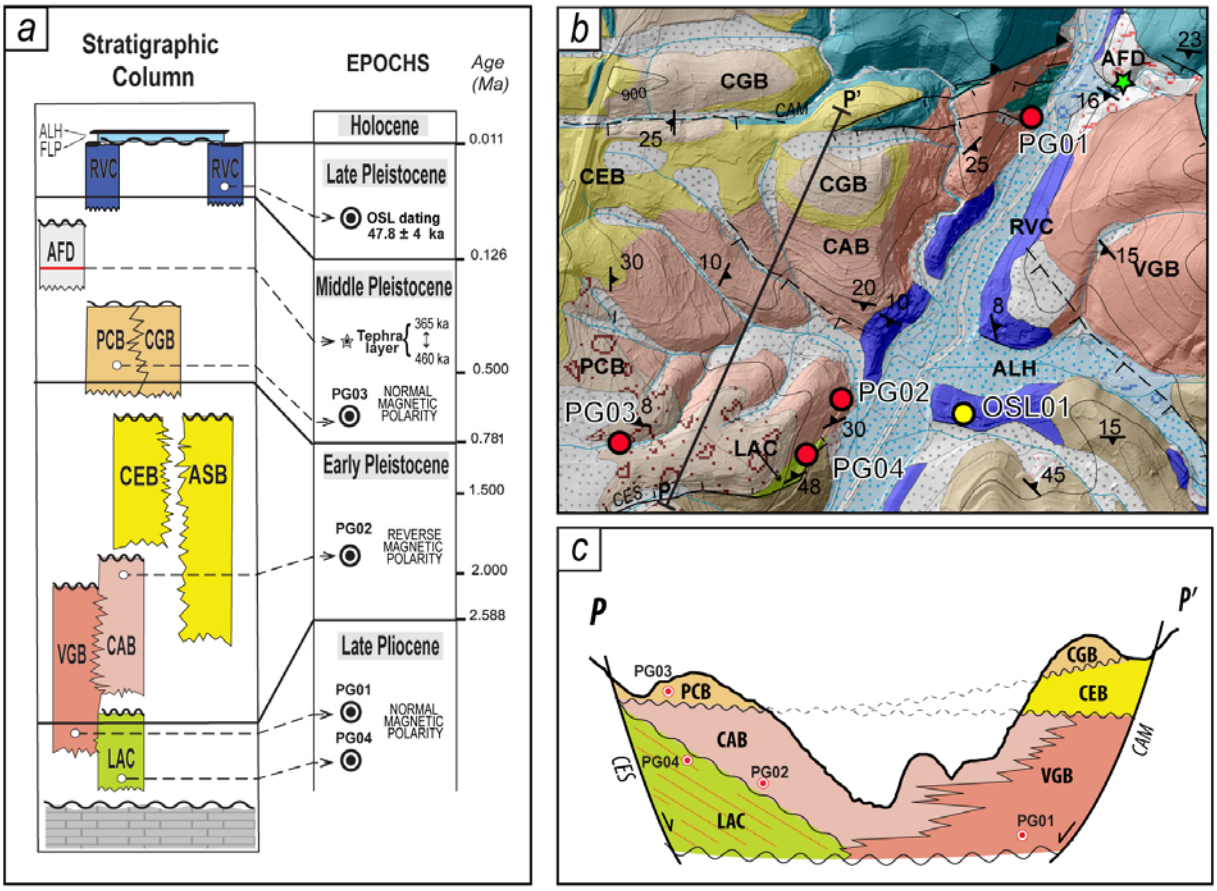

Figure 5. (a) Stratigraphic column of the Quaternary deposits in the study area (modified after Pucci et al., 2019); in the panel, the paleomagnetic and OSL dating are indicated, along with the reworked tephra found within the AFD deposit and possibly correlated with those from Giaccio et al. (2012). (b) Geological map of the Camarda basin (location in Fig. 3) with the attitude of the depositional bodies and sampling locations indicated. (c) Schematic geological section PP' (location in panel b) shows different interfingering of depositional bodies.

Fluvial–alluvial deposits along the Raiale River valley are restricted along its incised channel. The oldest is the Ancient Fan Deposit formation (AFD Fm., Fig. 5), which hangs up to 90 m above the present-day river talweg, northeast of the Camarda village. It contains an extensive and well-preserved 40-cm-thick brown paleosol topped by a ~10-cm-thick reworked tephra layer (green star for location in Figs. 3 and 5), which can be roughly correlated to those found elsewhere in the L'Aquila area. In particular, tephra and volcanoclastic material were found in several sites close to the Paganica area and dated between 365 and 460 ka (correlated to the well-known eruptions of the

Latium volcanic districts; Giaccio et al., 2012). Thus, even though the tephra was not dated owing to its intense reworking, it can be reasonably assumed that it is not older than 460 ka. The terraced fluvial–alluvial deposits disconnected from the present-day Raiale River dynamics are reported as Raiale Valley Conglomerates formation (RVC Fm.; Figs. 3 and 5). They comprise clast-supported conglomerates composed of cross-stratified and imbricated coarse gravels, mainly from the carbonate Meso–Cenozoic sequence. RVC presents laterally continuous and well-defined subhorizontal treads, locally well-cemented, and erosional bases on bedrock or Quaternary sediments.

4.2 Geomorphology

4.2.1 Morphostratigraphy and Quaternary evolution

The vertical/lateral relationships among the clastic formations of the Camarda basin described in Section 4.1.1 are associated with depositional and erosional surfaces. Relative and absolute chronologies, altitudinal range, and morphological cross-cutting relationships between tectonic landforms and paleosurfaces were used to reconstruct the main phases of the morphotectonic evolution of the study area.

The confinement of the E–W elongated Camarda basin suggests a possible initial hydrological disconnection from the proto-MAV basin, as hypothesized for similar basins by Geurts et al. (2020). Its infilling, comprising LAC, CAB, and VGB Fms., is topped by a paleosurface, suspended at ~950 m a.s.l. and related to the ancient phases of relief smoothing, associated with the deposition of CEB and the ASB breccia Fms. (Figs. 6 and 7). This gently rolling landscape (after this Cesarano paleosurface) runs along the Raiale River's right-hand side and is inset in the high-standing low-relief surface carved on the Meso–Cenozoic substratum of Mt. d'Aragno. This paleolandscape resembles a NE–SW-elongated paleovalley, suggesting the occurrence of a proto-Raiale valley standing at higher elevations (from ~175 to 205 m) above the present-day Raiale River talweg (Figs. 3 and 6). The

Cesarano paleosurface correlates with the erosional surface of Collalto (~975 m a.s.l.) on the Raiale River's left-hand side (Fig. 6). A depositional surface of PCB Fm. and CGB Fm. unconformably lays at an elevation of 875 m a.s.l (after this Cesarano plain), possibly displaced by E-trending normal faults.

Such landscapes are deeply incised by the Raiale River, which cuts a deep gorge connecting the Assergi basin to the Paganica-San Demetrio basin (Figs. 6 and 7). At the Raiale River outlet a large Holocene alluvial fan developed within the dissected Early–Middle Pleistocene terraces.

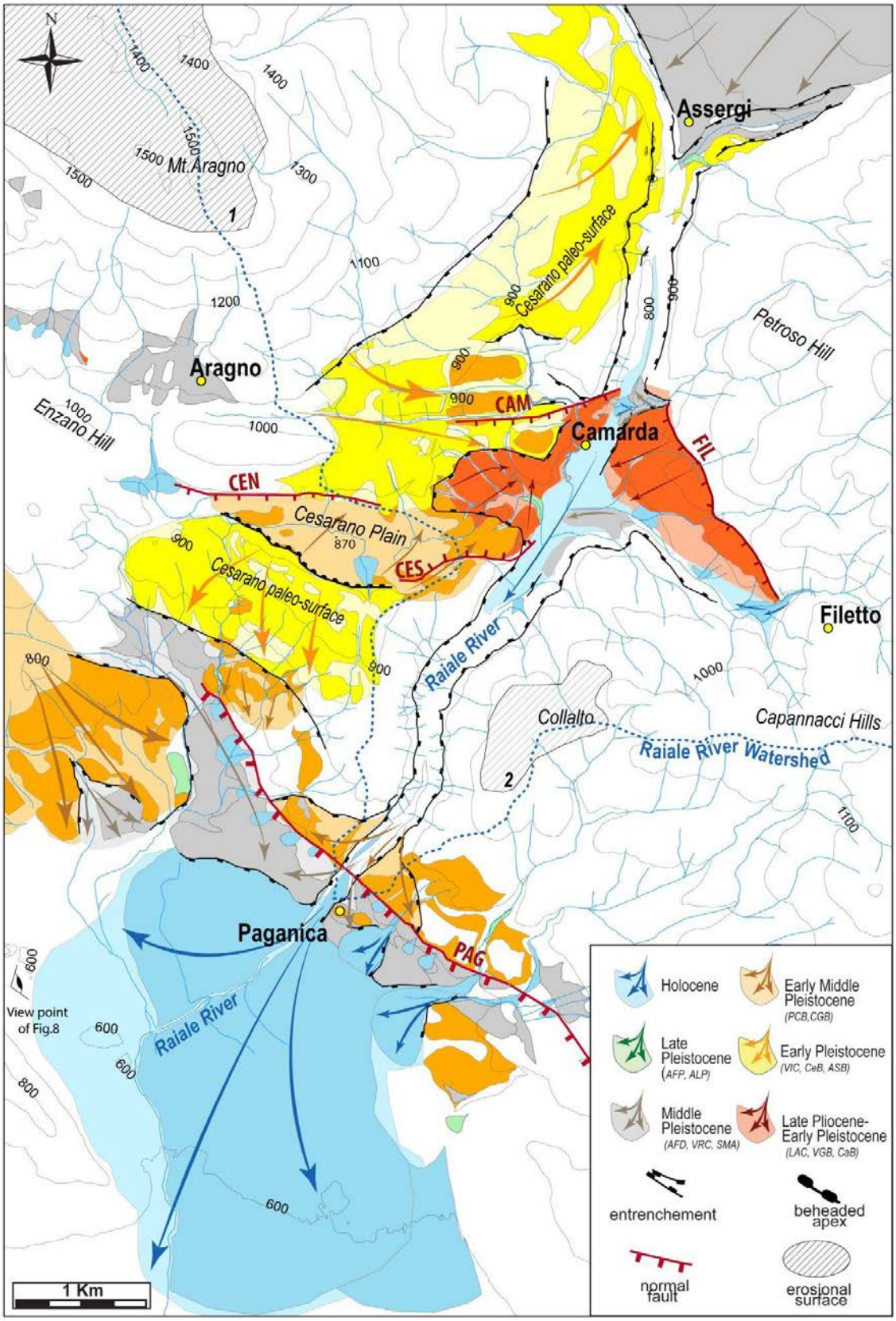
N
Assergi
Mt.Aragno
1
Aragno
Enzano Hill
Cesarano paleo-surface
Petroso Hill
CAM
Camarda
FIL
CEN
Cesarano Plain
870
CES
Cesarano paleo-surface
Filetto
Raiale River
Collalto
2
Capannacci Hills
Raiale River Watershed
Paganica
PAG
Raiale River
View point of Fig.8
1 Km
Holocene
Early Middle Pleistocene (PCB,CGB)
Late Pleistocene (AFP, ALP)
Early Pleistocene (VIC, CeB, ASB)
Middle Pleistocene (AFD, VRC, SMA)
Late Pliocene-Early Pleistocene (LAC, VGB, CaB)
entrenchement
beheaded apex
normal fault
erosional surface

447

Figure 6. Scheme of the cross-cut relationships among the continental bodies in the footwall of the Paganica fault. Light-colored polygons represent the hypothetical original depositional body extent. Dark-colored polygons are the depositional bodies outcropping in the field, and arrows indicate the main inferred paleoflow directions. The Paganica, Filetto, and Cesarano normal faults, the main body entrenchments, and the beheaded apexes are reported (modified from Pucci et al., 2019). Erosional surfaces are indicated.

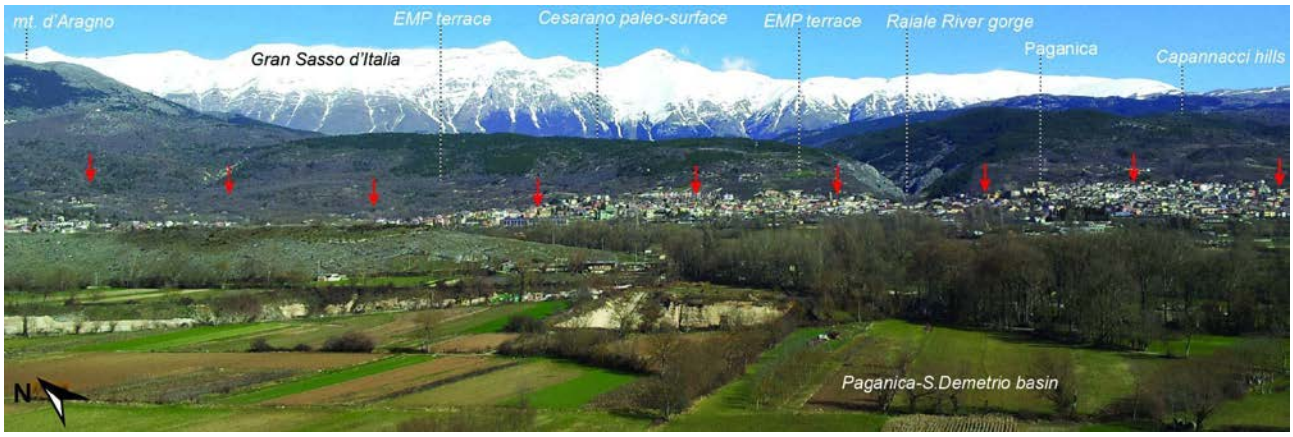

Figure 7. View of the Raiale River outlet and the Paganica-S.Demetrio basin, where its Holocene alluvial fan develops (viewpoint in Fig. 2). Red arrows point to the main PAG surface trace affecting the Early–Middle Pleistocene terraces (EMP). The gorge notably incises the hanging upper Cesarano paleosurface (in frontal view). In the background, the Gran Sasso Range watershed of the Raiale River is visible.

4.2.2 Present-day Raiale River longitudinal profile

The present-day Raiale River, mainly fed by the Gran Sasso Range water discharge, is ~17 km long and has a catchment of 106 km^2 with an asymmetric shape. Its path is almost rectilinear and shows an abrupt flow direction change from ESE, in the Assergi basin, to SSW from the Assergi Village, crossing the PAG (Fig. 8a).

The longitudinal profile of its main stem is characterized by three different sections separated by two knickzones: the upstream concave-up profile (up to 4000 m downstream distance) with a K_{sn} of 85.4 (see Supplementary Material A4 for major details); the intermediate section that shows a slight concave-up profile has a K_{sn} of 85.9) (between the Assergi and Paganica basins); the concave lower reach (from just upstream the PAG fault to the local base level of the Paganica-San Demetrio basin) shows a K_{sn} of 100 (Fig. 8b).

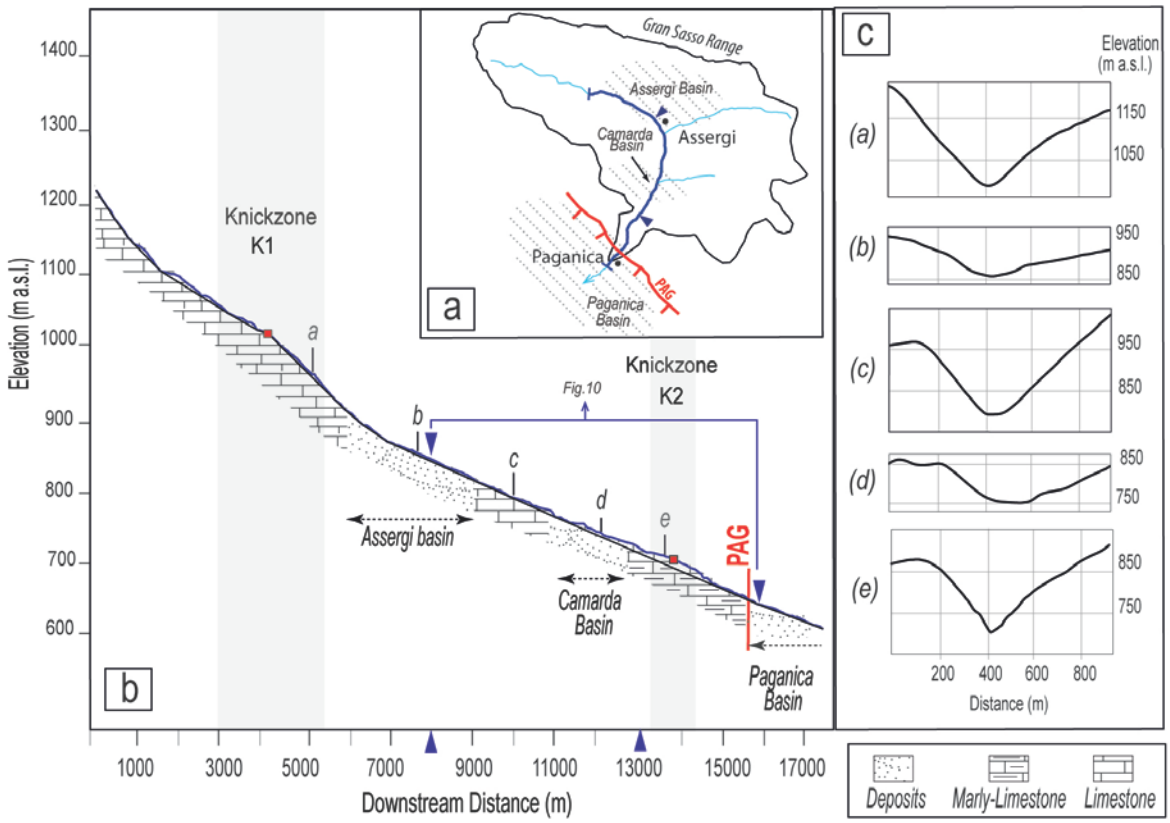

Figure 8. (a) Sketch of the Raiale River Watershed and the main drainage lines crossing the three basins of Assergi, Camarda, and Paganica; (b) longitudinal profile of the Raiale River main trunk (dark blue in panel a). The two principal knickzones, K1 and K2, and the talweg type (bedrock vs. alluvial deposits) are indicated. Vertical exaggeration is 2×; (c) cross-valley profiles (see location in panel b). Vertical exaggeration is 2×.

Consequently, a first knickzone (K1) is located upstream of the Assergi basin, ~10 km from the PAG fault, and shows a convex profile at a downstream distance between 4,000 and 6,000 m (Fig. 8b). A second knickzone (K2) is located downstream, ~1500 m, before the PAG fault trace, where the longitudinal profile slightly increases in slope, showing a convexity between 13,000 and 14,000 m (Fig. 8b).

The Raiale River main stem in the PAG footwall mainly shows a bedrock talweg, dominated by detachment-limited (sensu Tucker and Whipple, 2002) erosional processes and associated with V-shaped cross-valley profiles (Fig. 8c). The bedrock talweg is composed of marly limestones (SCC-CRR Fms.) and limestones (COI-SCZ Fms.) with slightly different erodibility that does not control

483 the knickzones (Fig. 8b). When the talweg runs into thin alluvial deposits of the Assergi and Camarda
484 basins, the cross-valley profiles widen and flatten (profiles b and d, Fig. 8c). In the proximity of the
485 PAG footwall knickzone K2, a deep gorge develops in bedrock, with valley-side cliffs (up to ~100 m
486 high) and very narrow bedrock valley floor, suggesting significant rejuvenation by fluvial incision
487 (profile e, Fig. 8c).

488 **4.2.3 Fluvial terraces along the Raiale River valley**

489 Along the Raiale River valley, between the Assergi and Paganica basins, flights of fluvial terraces
490 were recognized and mapped (Supplementary Material A3). Over 60 terrace treads were identified
491 and outlined by both inner and outer edges. Apart from a few cases, most of the fluvial terraces
492 (composed of RVC Fm., Fig. 3) are unpaired and show a strath-terrace nature, being very thin (<3–4
493 m). They lie a few meters (~5 m) above the present-day talweg in the Assergi basin while reaching
494 up to 80 m immediately north of the Paganica basin. Owing to the limited thickness and clear-cut top
495 of the deposits, the elevation difference was considered between the treads of the fluvial terraces
496 flights as a reliable expression of the elevation change instead of that calculated from their erosional
497 base (i.e., strath).

498 In the Camarda area, terraces tend to be more preserved with broad surfaces than those along the
499 valley because of a tributary from the left side (Fig. 6). In fact, along the steep V-shaped valley flanks,
500 hillslope processes dominate and terraces are likely to be less maintained (Fig. 8). Here, fluvial
501 deposits comprise small, terraced remnants with scarce to poorly preserved margins because of slope
502 processes that erode the outer risers or cover the inner edges with colluvial wedges.

503 Based on their continuity, average elevation range, and talweg-related elevations (i.e., topographic
504 difference with the present-day Raiale River as baseline), the correlation of five terrace orders was
505 possible through a linear regression (Fig. 9). In particular, if the population of terraces at distances of

8,000–9,000 m is considered, the talweg-related elevations for each terrace order are as follows: order I, 38.5 ± 11 m; order III, 21.3 ± 3 m; order IV, 10.9 ± 3 m; and order V, 3.5 ± 1 m. The same terrace orders at downstream distances of 11,500–12,500 m have the following elevation: 66.9 ± 10 m for the order I; 35.5 ± 1 m for order III; 25.9 ±3 m for order IV; and 13.1 ± 7 m for order V, the youngest terraces. An order II of terraces, having a limited extent through the River Valley, is found from 9,500 to 11,300 m with elevations over the talweg from 22.7 ± 1 to 31.1 ± 3 m. Hence, the talweg-related elevations of each terrace order increase downstream. This evidence denotes a positive gradient in the incision rate approaching the PAG fault.

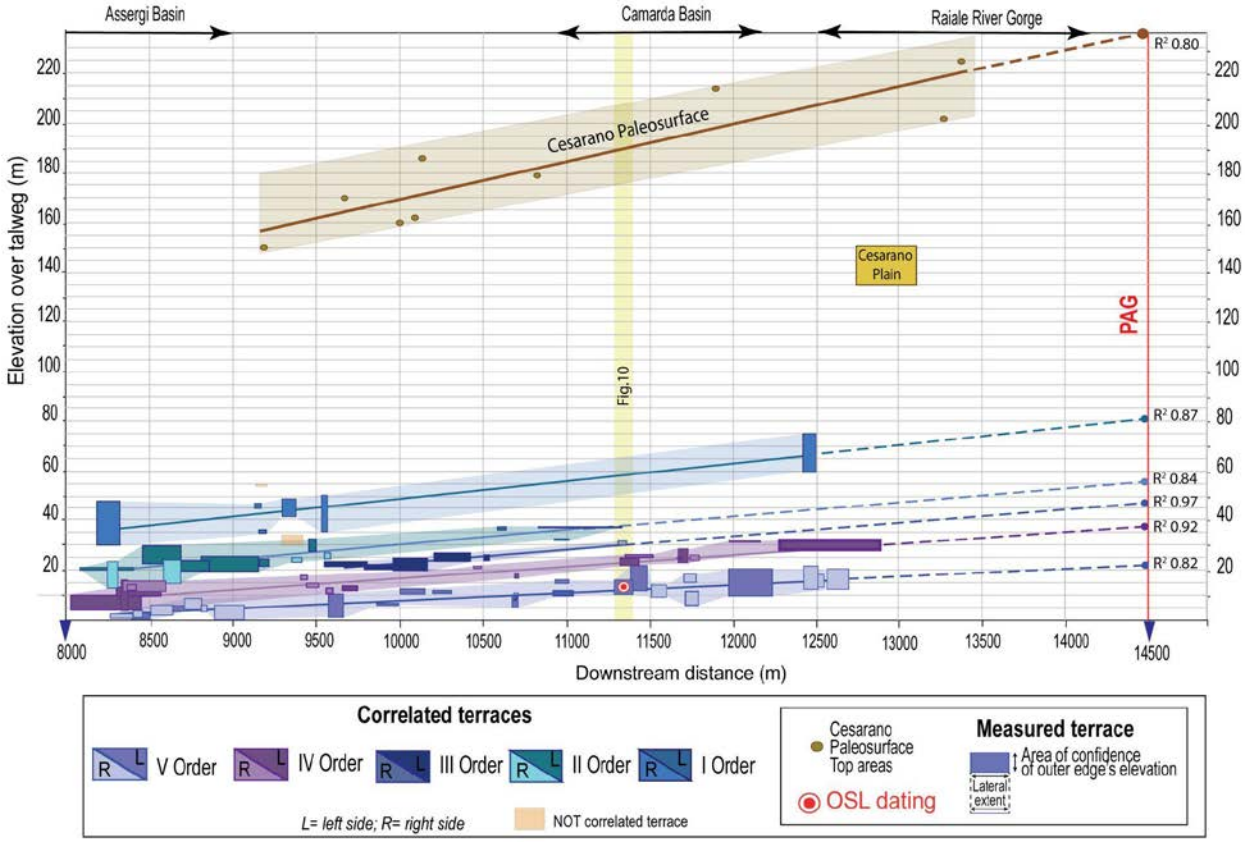

Figure 9. Projected longitudinal profiles of the elevations of river terraces along the two sides of the Raiale River present-day talweg (see Fig. 9a for the baseline location). The solid boxes describe the elevation range of the outer edges. The box width accounts for the lateral extent of each detected terrace. The box height points to the elevation uncertainty (measured at the beginning and end of each terrace edge). The correlation (linear regression line) of the average elevation for each terrace order is reported as a solid line and its projection on the PAG fault is reported as a dashed line. The

correlation coefficient of each order of terraces is also indicated. All the elevations are relative to the zeroed talweg. Elevation points measured at the top areas of the Cesarano Paleosurface and elevation of the Cesarano plain are also reported. Light-colored areas indicate the range of elevation of each dataset group (i.e., terrace order and paleosurface).

4.4 Incision and erosion rate estimate

The five orders of fluvial terraces recognized along the upper reach of the Raiale River were crucial to estimating incision rates, which were subsequently compared to denudation rates obtained for the low-relief uplands of the drainage basin.

4.4.1 Paleolongitudinal profile age and incision rates

At an elevation of 12 m from the talweg, the terrace order V close to the Camarda village was sampled (distance 11,300 m, Fig. 9), where the terrace is well-preserved and continuous with a thickness of ~10 m. The OSL analysis provided an age of 47.8 ± 4 ka for the terrace order V (Tab. 1). Considering its talweg-related elevation, an incision rate of 0.25 ± 0.02 mm/a for the youngest paleolongitudinal profile of the Raiale River at the sampling point was determined.

OSL ID	Lab	Grain size Ø (µm)	ED (Gy)	DR (mGy/h)	Age (ka)
CAM1	Ph3dra-INFN	180–212	70.8 ± 5.8	1.48 ± 0.3	47.8 ± 4.0

Table 1. Results of the OSL analysis. All errors are at one sigma except for ED (two sigma). See Figs. 3 and 4 for locations.

Assuming a relatively constant incision rate of 0.25 ± 0.02 mm/a over the Pleistocene, the possible age range of the terrace flights from their talweg-related elevation at the sampling point can be inferred (Fig. 10). Afterward, their possible match with favorable climatic stages was checked by correlation with the OIS curve (Lisiecki and Raymo, 2005) considering that their worldwide cyclic formations might have been a response to climatic fluctuations (Bridgland and Westaway, 2008).

Starting from the dating age of the terrace order V tread, whose deposition occurred at the OIS 3/4, the sequence of the terrace orders IV, III, II, and I can tentatively be correlated with OIS 5c/d, 5d/6, 6, and 8, respectively. The evidence that the obtained ages of these fluvial terraces fit well the aggradation processes that occurred during glacial periods further supports our hypothesis of a fairly constant incision rate through time. The fluvial terraces appear to be preserved starting from 300 ka ago.

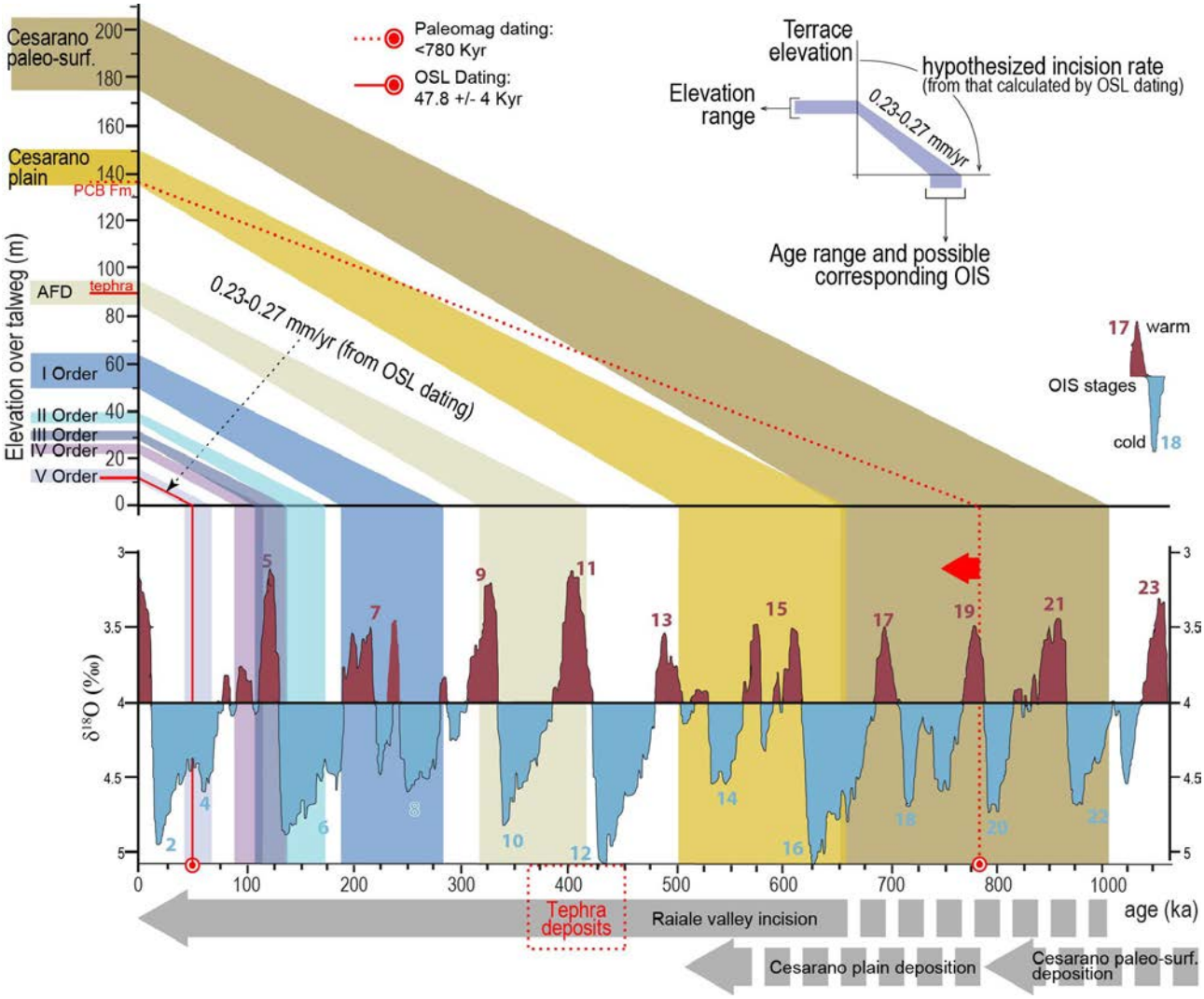

Figure 10. Correlation of the Raiale River terrace distribution and Cesarano paleosurface with the OIS time curve of Lisiecki and Raymo (2005). The incision rate estimated from the V terrace order OSL dating is reported and applied for correlating the river terrace orders and paleosurface elevation with the isotopic time curve. The correlation applies to the OSL sampling point (see Fig. 9 for the location along with the Raiale River longitudinal profile).

The same incision rate of 0.25 ± 0.02 mm/a assigned to the Ancient Fan Deposit formation (AFD Fm, Fig. 3), which contains the reworked thick tephra layer and hangs up to 90 m above the nearby present-day river talweg, matches quite well the period of tephra deposition that occurred in the area before 460 ka ago (Fig. 10).

Similarly, if a constant incision rate of 0.25 ± 0.02 mm/a is assumed since the onset of the Raiale River all along the main stem, an age for both the Cesarano paleosurface and the Cesarano plain dissections can be inferred. The Cesarano plain stands at ~135–150 m above the talweg (Fig. 9), and its estimated incision onset is in the range of 500–655 ka. This age agrees with the upper age limit of 780 ka, constrained by the magnetic polarity of the PCB Fm. deposits forming the reference plain (Fig. 10). Meanwhile, the Cesarano paleosurface stands at ~175–205 m above the talweg, and the inception age of its downcutting could be 0.65–1.0 Ma (Fig. 10).

4.4.2 Denudation rates from terrestrial cosmogenic nuclides (TCN)

For the denudation rates estimation of the summit with in situ produced terrestrial cosmogenic nuclide ^{36}Cl (TCN), a sampling at low-relief uplands (1200–1550 m a.s.l.) in the vicinity of the Raiale River's watershed was conducted (Fig. 2). The RA-E02, RA-E03, and RA-E01 samples were collected from Cretaceous limestones. Sampling locations were on the Mt. d'Aragno top, at the easternmost side of the Raiale watershed and on the divide between the Stabiata and the Collebrincioni basins. In addition, the RA-E04 sample was collected from Jurassic limestones on the Capannacci Hills.

Name	Long	Lat	Altitude (m)	mCa/ m rock dissolved [g/g]	CaO [%]
RA-E01	13.4152	42.4080	1283	0.23 ± 0.002	32.2
RA-E02	13.4594	42.4105	1548	0.393 ± 0.004	55.1
RA-E03	13.5466	42.3904	1448	0.463 ± 0.003	64.8
RA-E04	13.5234	42.3612	1206	0.398 ±0.003	55.6

571 **Table 3.** Sample location and the amount of calcium in the samples. See the main text for a description.

572 From the 3-cm-thick rock samples (density of 2.7 g/cm^3), the ^{36}Cl concentrations were determined.
573 The number of neutrons and muons found in each sample and the related grams of Ca/CaO in the
574 dissolute rock sample are shown in Table 3. The measured ^{36}Cl amount ranges from 1.37×10^8 to
575 2.22×10^8 atoms (Table 2), three orders of magnitude higher than that measured in the blanks ($1.52 \times$
576 10^5 atoms of ^{36}Cl). The measured amount of natural chlorine (Cl-$_{nat}$) in the samples is 2–3 orders of
577 magnitude higher than that of blank: it ranges between 2.6×10^{20} and 6.6×10^{19} atoms versus the $2 \times$
578 10^{17} atoms in the blank. Using the Schimmelpfennig et al. (2009) spreadsheet and corrections for
579 altitude and latitude from Stone (2000), the denudation rates of the samples were determined (Table
580 4).

581 The values clustered around 24–44 m/ka. The lowest value is from the RA-E02 sample located at the
582 highest elevation, while the others give similar results. The mean denudation rate at the footwall of
583 the Paganica normal fault, calculated from TCNs, is 0.02–0.04 mm/a.

Name	n(^{35}Cl)/n(^{37}Cl)	Atoms Clnat (x 10^{19})	Atoms ^{36}Cl (x 10^{8})	Atoms $^{36}Cl_{corr}$/g of rock (x 10^{6})	Denudation Rate (m/ka)
RA-E01	3.64 ± 0.01	26.1 ± 0.69	2.22 ± 0.08	3.14 ± 0.1	40.8 ± 4
RA-E02	5.07 ± 0.02	6.89 ± 0.10	1.60 ± 0.05	2.07 ± 0.08	23.6 ± 2
RA-E03	5.12 ±0.02	6.70 ± 0.12	1.46 ± 0.05	1.96 ± 0.07	43.7 ± 4
RA-E04	5.08 ±0.03	6.93 ± 0.14	1.37 ± 0.05	2.21 ± 0.08	36.1 ± 3

584 **Table 4.** Accelerator mass spectrometry measurements of the ^{35}Cl/^{37}Cl ratio, the number of atoms of Cl_{nat} and ^{36}Cl, and
585 the corresponding atoms of ^{36}Cl per gram of rock. The denudation rate (mm/a) is determined with the Excel spreadsheet
586 of Schimmelpfennig et al. (2009). See the main text for a description.

587 **5.1 Plio–Pleistocene evolution of the area**

588 By integrating stratigraphic, morphotectonic, and paleomagnetic data, a Quaternary evolution model
589 of the studied area was proposed, composed of four different stages that led to the emplacement and
590 development of the Raiale River in its current form.

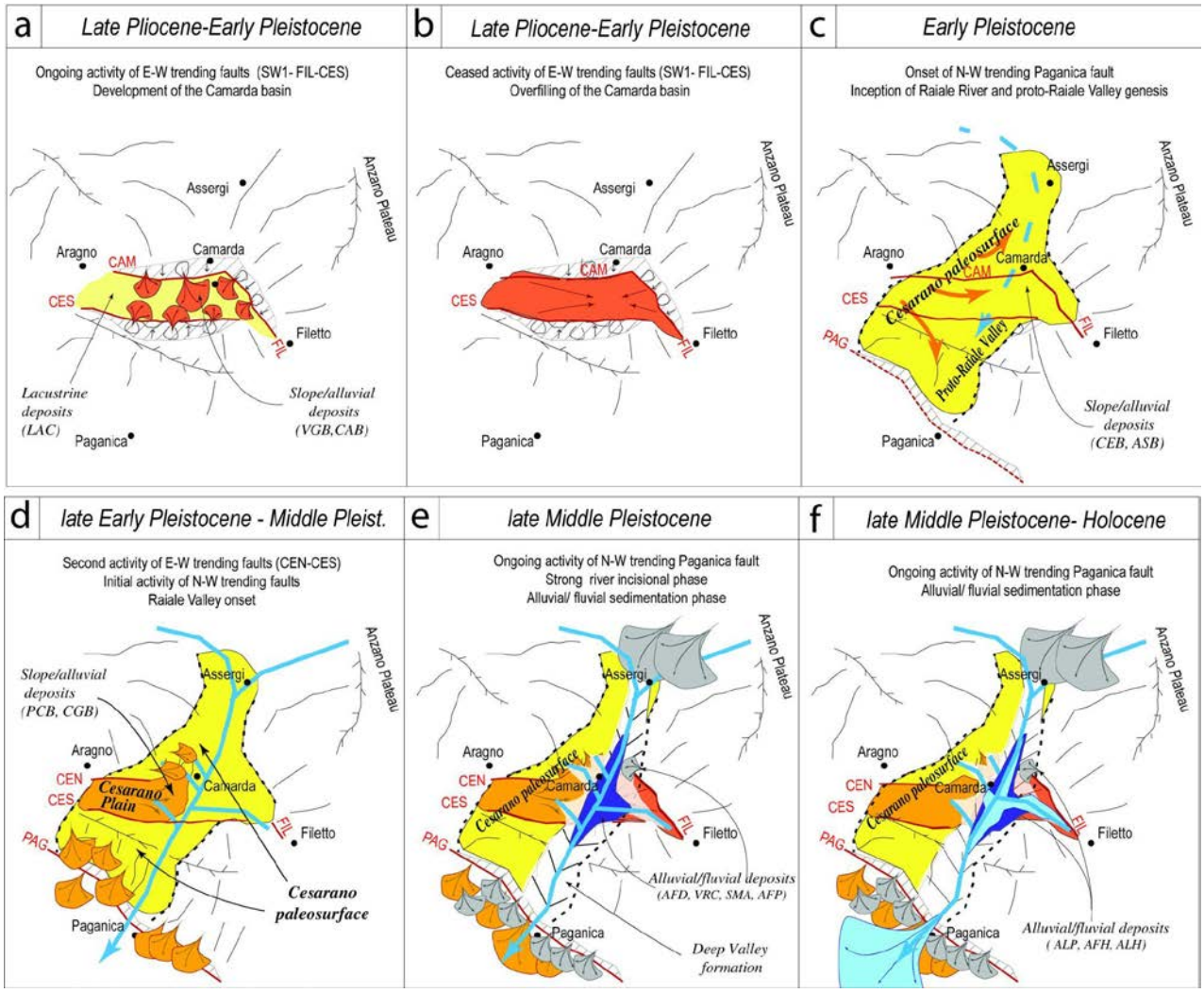

Figure 11. Sketch of the evolution of the Raiale River studied area from the Late Pliocene to the Holocene. See the main text for details.

(1) Late Pliocene–Early Pleistocene. In the Late Pliocene, the development of E–W- and NNW–SSE-trending fault systems occurred, in agreement with the evolution model proposed for the MAV by Pucci et al. (2019). These fault systems led to the genesis of the Camarda tectonic satellite basin, E–W elongated and narrow, isolated by structural bedrock highs. The Camarda depositional sequence unconformably lying on the Meso–Cenozoic substratum is composed of an early lacustrine deposition (LAC), followed by confined bodies of breccia (VGB and CAB) that progressively infilling the basin (Fig. 11 a-b). Notably, in the study area, based on the normal polarity of paleomagnetic data, the lacustrine deposition occurred starting from the Pliocene. Lacustrine deposits possibly result coeval

602 with the Late Pliocene onset of the lacustrine depositions of the San Nicandro Fm. in the MAV basin
603 (Spadi et al., 2016; Pucci et al., 2019). After increasing the syn-rift topographic relief, an Early
604 Pleistocene environmental change led to high-energy deposit production and slope debris/breccia
605 deposition in dry or transport-limited conditions. The evidence of numerous syntectonic depositions
606 denotes a long-lasting activity of the basin-bounding E–W-trending normal faults.

607 This initial phase predates the Raiale River gorge's incision, as testified by the breccias paleoflow
608 and bedding dip directions converging to an E–W oriented depocenter, which is now disjointed from
609 the present-day morphodynamics.

610 (2) Early Pleistocene. A depositional phase of breccia deposits (CEB/ASB Fms.) showing reverse
611 paleomagnetic polarity, has filled to the brim the Camarda basin and has covered with a marked
612 angular unconformity the shallow-dipping CAB and VGB Fms. The deposition drapes a wide NE–
613 SW-trending paleovalley, inset between Mt. d'Aragno and Capannacci Hills, forming the early
614 connection between the Assergi and the Paganica basins (Fig. 11c). Its geometry suggests a landscape
615 influenced by the paleodrainage activity of the proto-Raiale River. The deposition's lack of distal
616 alluvial facies is possibly due to the immature drainage catchment and prevalent supply from high-
617 gradient slopes. The present-day gentle NE-sloping of the paleovalley can be related to the postEarly
618 Pleistocene footwall back-tilting due to the intervening PAG activity.

619 (3) Late Early Pleistocene–Middle Pleistocene. Entrenchments locally start to interrupt the lateral
620 continuity of the Cesarano land surface (Fig. 11d). Limited breccia bodies (PCB and CGB Fms.)
621 prograde toward the paleo-Raiale River and infill inset E–W-elongated, fault-controlled narrow
622 basins. It can be inferred that the Cesarano plain was modeled at ~500–650 ka from the estimated
623 constant incision rate.

The limited dissection of the Cesarano paleosurface suggests a reduced activity of the E–W-trending normal faults (e.g., CES, CEN, and SW faults). At the end of this phase, the Raiale River starts to incise the Cesarano paleosurface (Fig. 10 and 11e). This latter testifies to an ongoing PAG activity that progressively lowered the Raiale River base level (i.e., the Paganica-San Demetrio basin, on the hanging wall), hanging the Cesarano paleosurface up to >200 m above the present-day talweg.

(4) Late Middle Pleistocene–Holocene. The activity of the PAG continues to trigger the headward erosion of the Raiale River drainage and the deepening of the longitudinal profile at its footwall. Concurrently, stadial and interstadial phases drive the formation of a set of fluvial terrace flights, inset into the Raiale River valley, progressively disconnects from the stream dynamics (Fig. 11f).

The incision record documented for the Raiale River valley suggests its inception at the Late Early Pleistocene-beginning of the Middle Pleistocene (Fig. 10). This is in agreement with (1) the increased activity of the NW–SE-trending normal faults (Pucci et al., 2019) that, according to some authors, is due to the fault linkage acceleration invoked for this sector of the Apennines (Roberts and Michetti, 2004; Whittaker et al., 2007b; Whittaker et al., 2008); (2) the timing of the drainage integration of the Paganica-S.Demetrio basin into the regional Aterno River system (0.7–0.8 Ma) (Geurts et al., 2020); and (3) reduction in sediment supply at the end of the Mid-Pleistocene climatic transition (0.7–1.25 Ma) (Whittaker et al., 2010; Whittaker and Boulton, 2012; Head and Gibbard, 2015; Willeit et al., 2019).

5.2 River incision and long-term slip rate from the Paganica fault footwall

A graded theoretical profile (for details, see A4 in Supplementary Materials) that connects the local base level (i.e., Paganica-San Demetrio Basin) with the upper reach (p3) suggests the equilibrium talweg to which the Raiale River would tend in the absence of perturbations (Fig. 12). Conversely, the Raiale River longitudinal profile is interrupted and subdivided into different sections by

knickzones k1 and k2, denoting an ungraded status. Therefore, the different sections of the present-day Raiale River longitudinal profile (Fig. 8b) can be extrapolated downstream to represent their theoretical equilibrium. The graded upstream concave-up profile (p1) hangs above the Raiale River talweg up to ~250 m approaching the PAG fault (Fig. 12), mimicking the suspended Late Early Pleistocene Cesarano paleosurface elevation trend (Fig. 5a, 6, and 9); the more rectilinear intermediate section (p2), which is characterized by the presence of the river terrace flights, is projected over the Raiale River outlet at ~50 m.

Assuming these knickzones are not lithologically controlled, they constitute perturbations of the Raiale River profile, which respond to external base-level changes that must be communicated upstream until the whole catchment eventually reaches a new steady state topography. Such knickzones propagate through episodes of transient regressive erosion that adjust the longitudinal river profile (Pazzaglia et al., 1998; Whittaker et al., 2007a and 2007b).

The knickzone k1 appears to mark the upstream extent of the headward propagating incision wave affecting the Cesarano paleosurface. Considering its age of ~1.0 Ma and the ~12-km horizontal distance from PAG, an average migration rate of ~12 mm/a is found, similar to that found by Whittaker et al. (2008) in response to active faulting in the Central Apennines. Furthermore, the well-preserved knickzone k1 could represent the transient landform (i.e., *not* in a topographic steady state) probably triggered by the new tectonic forcing before the Middle Pleistocene.

Similarly, the knickzone k2 at the intermediate Raiale River longitudinal profile marks the incision wave affecting section (p2) near the PAG fault. The resulting convexity represents a transient landform that indicates a younger perturbation (applying the k1-derived migration rate could have around 125 ka), possibly related to the increase in footwall uplift, the decrease in water discharge

(following the last interglacial period), and the lithological control of the Raiale bedrock gorge compared to the Paganica-S. Demetrio basin.

Certainly, the intermediate Raiale River longitudinal profile, upstream of k2, presents hanging paleolongitudinal profiles depicted by five orders of strath terraces (Figs. 9 and 12). These paleolongitudinal profiles diverge downstream. Such a divergence indicates a footwall uplift gradient approaching the PAG fault, invoking a tectonic control for the present-day longitudinal profile.

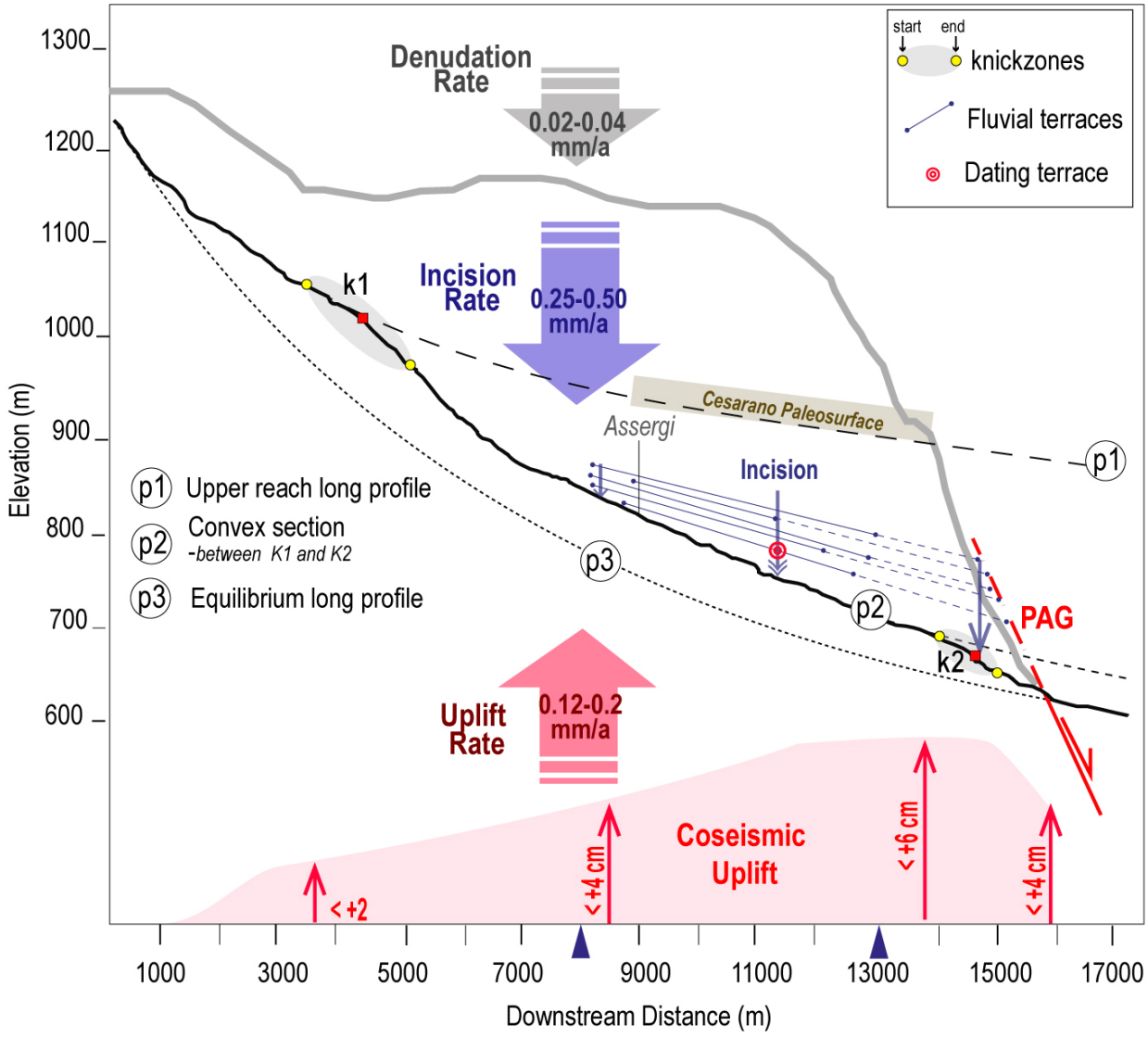

Figure 12. Conceptual sketch of the Paganica Fault footwall evolution (vertical exaggeration) showing the competition between local tectonic forcing, incision, and denudation rate along the Raiale River longitudinal profile. The upper reach long profile is p1, derived by the concave equilibrium profile from the portion up to k1, and it coincides with the Cesarano paleovalley. The convex section p2 is related to the longitudinal profile portion between the two knickzones. The equilibrium profile p3 is derived by interpolating the profile shape at the hanging-wall of the PAG and the starting point of the Raiale River (0 m downstream distance). Denudation rate comes from the TCN method; incision rate derives from fluvial terrace analysis; the profile of the coseismic vertical dislocation along the Raiale River (from the DInSAR data of Atzori et al., 2009; Fig. 13); uplift rate is based on the coseismic uplift (up to 6.0 cm) over the average recurrence time (300–500 years, from paleoseismological data) (see the text for explanation).

In this context, the incision rate of the Raiale River is strictly connected to the capability of the drainage system in contrasting the tectonic uplift and adjusting to the new base-level conditions (i.e., PAG hanging wall subsidence). Considering that a steady-state downcutting of the uplifting footwall is not reached and the Paganica alluvial fan aggradation sustains the concave-up profile (p3) at the subsiding hanging wall, the incision rate of the Raiale River can give a minimum estimate of the PAG throw rate.

The hypothesis of a constant incision rate along the entire stem can be misleading (e.g., Zhang et al., 2018), although the considered assumptions include probable oscillations in the incision rate uncertainties. In fact, the proposed timing of the Raiale River valley evolution (Fig. 10) agrees with the stratigraphic framework reconstructed for the Camarda basin (Fig. 5) so that the incision rate estimate of 0.25 ± 0.02 mm/a seems reliable.

This value of the incision rate is calculated at 3 km from the PAG trace (Fig. 9), thus representing a fraction of the higher rate that is expected in the PAG proximity. To consider the increasing difference in elevation approaching the fault, by projecting the correlated terrace flight on the fault plane at an elevation of 21 m (Figs. 9 and 12), a minimum throw rate of 0.44 ± 0.04 mm/a was estimated for the PAG. This rate obtained over the last 200 ka is similar to the throw rate suggested by Galli et al. (2010) during the last 0.5 Ma, while it is higher than the range of rates (0.1–0.4 mm/a) found for the PSDFS and referred to the time scales of 10^4–10^6 ka (Pucci et al., 2019). Nevertheless, the value is in the range of most of the data about the throw rates of the Apennines faults that show values generally

below 1.0 mm/a (Roberts and Michetti, 2004; Cinti et al., 2019), with some exceptions such as 1.3 mm/a for the Magnola fault (Benedetti et al., 2013).

5.3 Landscape dynamics

The long-term (last 300 ka from cosmogenic ^{36}Cl nuclides) denudation rate of 0.02–0.04 mm/a calculated for the area is similar to the current denudation rate estimates on limestone in northern Italy for the inland areas (i.e., 0.01–0.03 mm/a in Furlani et al., 2009) and the Mediterranean region (e.g., 0.03 mm/a in Siame et al., 2004), which have been correlated only to precipitation rates (Ryb et al., 2014). Moreover, these cosmogenic erosion rates, similar to those from the upland landscape in cool temperate climates (Heimsath et al., 2001; Phillips et al., 2006; Gunnell et al., 2013), are comparable to or slightly lower than average erosion rates from cosmogenic ^{10}Be concentrations in river sediments crossing land surfaces or in tectonically stable areas (Olivetti et al. 2012).

The presence of the fault seems to not influence the variation of these values that are small compared to the magnitude order of the fault slip rate (factor of 10^{-2}; see Ch. 2). Such a summit denudation is much slower than the incision of the Raiale River valley. This is also due to the slow retreat of knickzones (e.g., k1) and associated upland transmission of the transient response to the perturbations. In fact, in the study area, the landscape adjustment to a change in boundary conditions is still ongoing after 1.0 Ma, in the range of periods that may last thousands to millions of years as observed worldwide (Di Biase et al., 2015). Consequently, such upland low erosion rates are crucial in ensuring the survival of remnant landscapes preserved at low-relief high elevations (e.g., Anzano Plateau in Fig. 2).

In the specific framework of the study area, the dynamic equilibrium between topography and tectonics appears to not have been reached. Consequently, the landscape evolution at the PAG footwall in response to the tectonic activity is dominated by relief growth since the Raiale Valley

incision rate is one order of magnitude higher than the nearby summit denudation rate (0.25 mm/a *vs.* 0.03 mm/a). Thus, the incision is not equaled by the denudation, depicting a nonsteady state of the topography (Fig. 12). Moreover, along with the Early–Middle Pleistocene climatic transition, the increase in fault-related relief progressively intensified the sediment and water supply to the local base level (i.e., Paganica-San Demetrio basin), playing a role in the drainage integration through overspill mechanisms (Geurts et al., 2020).

Generally, this result confirms that dynamic equilibrium conditions are not met. However, its attainment would be possible considering the scale of the study area (i.e., topographic changes are scale-dependent and not precluded at the local scale of observation <100 km^2 or at time scales smaller than the significant climatic cycles of $<10^5$ years; e.g., Tucker and Whipple, 2002; Whipple and Tucker, 2002; Baldwin et al., 2003).

5.4 Paganica fault coseismic behavior and its long-term expression

In this framework, each coseismic uplift of the PAG footwall (i.e., instantaneous perturbation produced by an individual seismic event) produces a transient wave of regressive erosion that tends to grade the longitudinal river profile by propagating knickzones. If tectonically controlled, the knickpoint k2 and convex section (p2) indicate a persistent perturbation of the present-day Raiale River longitudinal profile. Specifically, the knickpoint suggests that during the interseismic periods after each coseismic uplift, the Raiale River cannot return at the same equilibrium profile gradient to reach a steady-state downcutting because of short earthquake recurrence time and/or large individual coseismic displacements.

Notably, the 2009 L'Aquila earthquake produced surface faulting with of ~15 cm and a coseismic dislocation field, measured using remote sensing data (Atzori et al., 2009), with a maximum footwall uplift of up to ~6 cm coinciding with the Raiale River valley long-term downcutting (Fig. 13). In this

framework, the 0.25–0.50 mm/a incision rate would be able to compensate for the 0.12–0.2 mm/a derived from the 2009-like seismic events occurring on the PAG with a recurrence time interval of 300–500 years (derived from 60 mm coseismic uplift from InSAR data and interevent time intervals from paleoseismological data). This suggests that the present-day anomaly of the Raiale River longitudinal profile, if of tectonic origin, would be produced by events larger than the L'Aquila one (as those documented by paleoseismological investigations with M > 6.5 and ~0.5 m of throw per event) and not by footwall uplift related to seismic events similar to the 2009 earthquake. Conversely, such an uplift rate due to the PAG activity would not be compensated by the 0.02–0.04 mm/a denudation rate at the summits, which is sufficient to imply a progressive tectonic increment of their absolute elevation (Fig. 12).

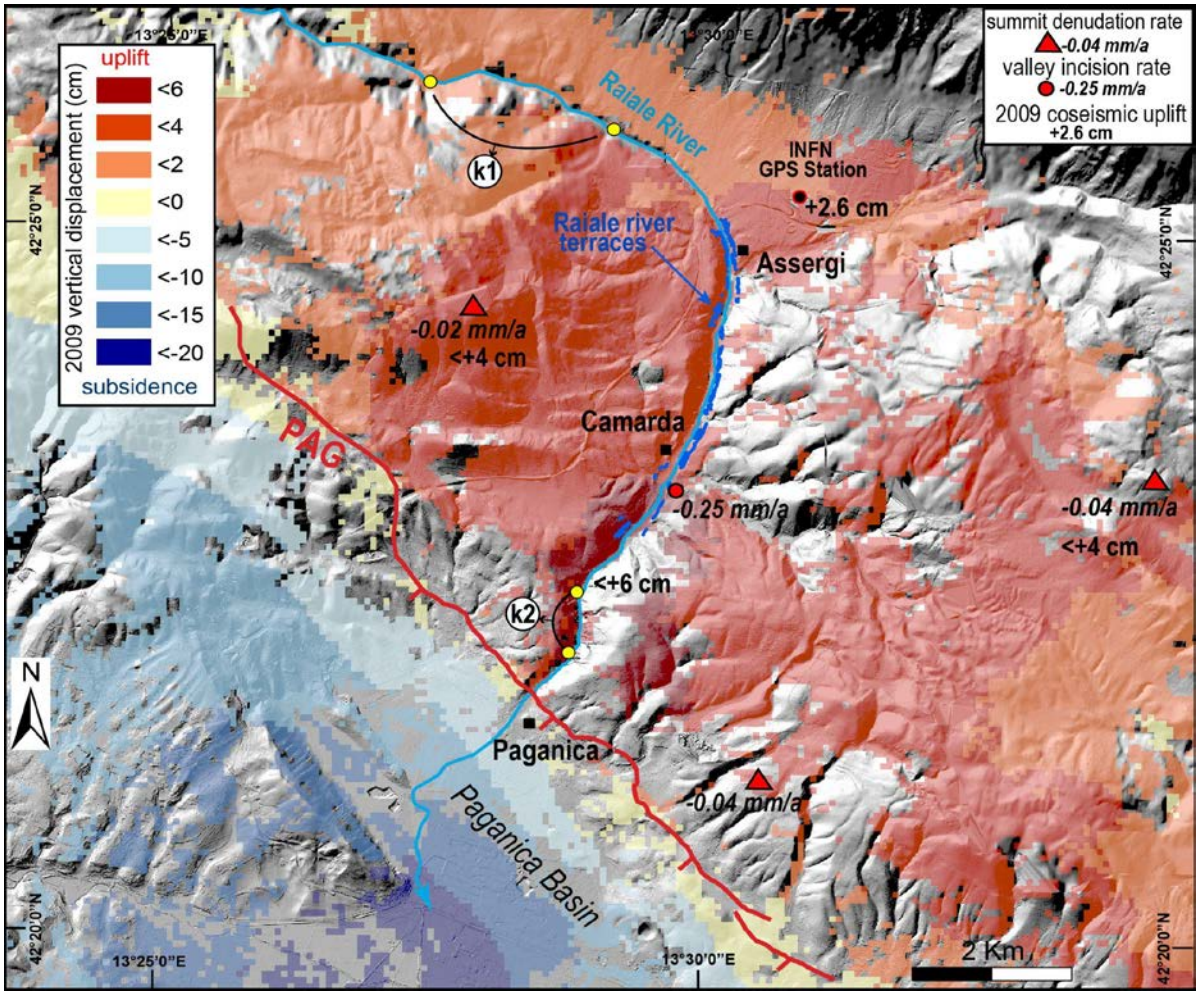

Figure 13. Vertical component of the 2009 coseismic observed displacement field from Envisat interferograms (Atzori et al., 2009) and the GPS station of INFN recorded an uplift of 2.6 cm (Anzidei et al., 2009). The footwall uplift maximum (6 cm) coincides with the portion of the Raiale River long profile corresponding with the p2 profile.

6. Conclusions

Herein, the footwall of the Paganica normal fault, the source of the 2009 Mw 6.1 L'Aquila earthquake in the Central Apennines, was investigated through integrated geological and geomorphological approaches and chronological data to extract constraints on active tectonics by taking advantage of the Raiale River that orthogonally crosscuts the fault trace. In particular, this work aimed to unravel the contribution of the Paganica normal fault activity in building the landscape and reconstruct its long-term throw rate by estimating and comparing denudation and incision rates at its footwall block.

Through morphostratigraphy and paleomagnetic analysis, we outlined the Plio–Pleistocene morphotectonic evolution of the area by reconstructing the spatially limited Camarda basin infill with its unconformity-bounded continental deposits and their relationships with faults. An initial phase of basin development was recognized that predates the Raiale River gorge's incision, controlled by dominant E–W trending faults in the Late Pliocene–Early Pleistocene and disjointed from the present-day Middle Aterno drainage. The following Early Pleistocene phase marks the superposition, by shaping and depositional draping, of the wide NE–SW-trending Cesarano paleovalley, forming the early connection between the Assergi and the Paganica basins. Afterward, during the Late Early Pleistocene–Middle Pleistocene, it starts the dissection of the Cesarano paleosurface with inset E–W-elongated paleosurfaces (i.e., Cesarano plain). At the end of this phase, the proto-Raiale River starts to incise these paleolandscapes severely, probably caused by an ongoing Paganica fault activity that progressively lowered the Raiale River base level. Up to the Holocene, the Raiale River strongly deepens its valley, leaving a set of fluvial terrace flights.

784 Detailed mapping of the Raiale River valley, along with absolute dating, allowed us to distinguish
785 five orders of Middle–Late Pleistocene fluvial terraces, from which paleolongitudinal profiles were
786 constructed, diverging downstream and depicting a footwall uplift gradient as approaching the
787 Paganica fault, consistent with long-term normal fault displacement. Consequently, we interpreted
788 the calculated 0.25 ± 0.02 mm/a incision rate as a minimum value for the near-fault footwall uplift,
789 where it can reach a throw rate of ~0.45 mm/a, in agreement with independent estimates derived from
790 the literature.

791 In parallel, through terrestrial cosmogenic nuclides, in 0.02–0.04 mm/a, the denudation rate on the
792 summit of the footwall block was calculated to be much slower than the incision of the Raiale River
793 valley. This result depicts a nonsteady state of the fault footwall topography, suggesting that the
794 dynamic equilibrium between topography and tectonics has not been reached; hence, a dominant
795 relief growth is expected.

796 In this framework, the present-day longitudinal profile of the Raiale River denotes an ungraded status,
797 presenting two main knickzones. The upper one results from the headward propagating incision wave
798 affecting the Cesarano paleosurface at the end of the Early Pleistocene and triggered by the Paganica
799 fault, showing an average migration rate in the order of 12 mm/a. The lower one, upstream of which
800 the diverging paleolongitudinal profiles are located, suggests a younger tectonic perturbation.

801 Finally, considering the L'Aquila earthquake coseismic dislocation field, it was observed that the
802 Raiale River incision rate estimated herein would be able to compensate for the maximum coseismic
803 footwall uplift if derived from 2009-like seismic events. This suggests that the present-day anomaly
804 of the Raiale River longitudinal profile, if it is a transient of tectonic origin, would have been produced
805 by larger events ($M > 6.5$) as those documented in the area by paleoseismological investigations.

This study provides a valuable case that demonstrates the usefulness of landform markers provided by interdisciplinary approaches of Quaternary geology, morphostratigraphy, and drainage analysis in quantifying postorogenic tectonic forcing in the Apennines from landscape response. It casts light onto the role of the activity of the Paganica fault by discriminating the landscape response to its footwall block dislocation, which is given by the river adjustment and the depositional/erosional processes and fault-controlled basins.

Moreover, the results confirm that in the Apennines, the condition of dynamic equilibrium is often not met, and that the persistence of transient perturbations induced by tectonics deserves consideration.

Acknowledgments

The work was financially supported by the MIUR (Italian Ministry of Education, University and Research) project “FIRB Abruzzo - High-resolution analyses for assessing the seismic hazard and risk of the areas affected by the 6 April 2009 earthquake”, ref. RBAP10ZC8K_005 and RBAP10ZC8K_007, and by Agreement INGV-DPC 2012-2021. Special thanks to Simone Atzori, who provided the InSAR data. Thanks to Riccardo Civico, Deborah Di Naccio, and Ari Matmon for the valuable discussions in the field and Chiara Caricchi for her help during the paleomagnetic analysis at the INGV laboratory in Rome. We also thank Alexander Whittaker, Alessandra Ascione and anonymous reviewer for their useful and perceptive comments that helped to improve the clarity and quality of the paper.

References

Ahnert, F. (1994). Equilibrium, scale and inheritance in geomorphology. Geomorphology, 11(2), 125-140.

828 Aitken, M. J. "Thermoluminescence dating: past progress and future trends." Nuclear Tracks and
829 Radiation Measurements (1982) 10, no. 1-2 (1985): 3-6.

830 Anzidei, M., Boschi, E., Cannelli, V., Devoti, R., Esposito, A., Galvani, A., Melini, D., Pietrantonio,
831 G., Riguzzi, F., Sepe, V., Serpelloni, E., 2009. Coseismic deformation of the destructive April 6,
832 2009, L'Aquila earthquake (central Italy) from GPS data. Geophys. Res. Lett. 36, 1–5.
833 https://doi.org/10.1029/2009GL039145

834 Atzori, S., Hunstad, I., Chini, M., Salvi, S., Tolomei, C., Bignami, C., Stramondo, S., Trasatti, E.,
835 Antonioli, A., Boschi, E., 2009. Finite fault inversion of DInSAR coseismic displacement of the 2009
836 L'Aquila earthquake (central Italy). Geophys. Res. Lett. 36, 1–6.
837 https://doi.org/10.1029/2009GL039293

838 Azañón, J. M., Azor, A., Pérez-Peña, J. V., & Carrillo, J. M. (2005). Late Quaternary large-scale
839 rotational slides induced by river incision: the Arroyo de Gor area (Guadix basin, SE
840 Spain). Geomorphology, 69(1-4), 152-168.

841 Bagh, S., Chiaraluce, L., De Gori, P., Moretti, M., Govoni, A., Chiarabba, C., ... & Romanelli, M.
842 (2007). Background seismicity in the Central Apennines of Italy: The Abruzzo region case study.
843 Tectonophysics, 444(1-4), 80-92.

844 Bagnaia, R., D'epifanio, A., & Sylos Labini, S. (1992). Aquila and Subequan basins: an example of
845 Quaternary evolution in Central Apennines, Italy. Quaternaria Nova, 2, 187-209.

846 Balasco, M., Galli, P., Giocoli, A., Gueguen, E., Lapenna, V., Perrone, A., Piscitelli, S., Rizzo, E.,
847 Romano, G., Siniscalchi, A., Votta, M., (2011). Deep geophysical electromagnetic section across the
848 middle Aterno Valley (central Italy): Preliminary results after the April 6, 2009, L'Aquila earthquake.
849 Boll. di Geofis. Teor. ed Appl. 52, 443–455. https://doi.org/10.4430/bgta0028

850 Baldwin, J.A., Whipple, K.W., Tucker, G.E., (2003). Implications of the shear stress river incision
851 model for the timescale of post-orogenic decay of topography. J. Geophys. Res. 108 (B3).
852 http://dx.doi.org/10.1029/2001JB000550.

853 Benedetti, L., Manighetti, I., Gaudemer, Y., Finkel, R., Malavieille, J., Pou, K., Arnold, M., Aumaître,
854 G., Bourlès, D., Keddadouche, K., (2013). Earthquake synchrony and clustering on Fucino faults
855 (Central Italy) as revealed from in situ36Cl exposure dating. J. Geophys. Res. Solid Earth 118, 4948–
856 4974. https://doi.org/10.1002/jgrb.50299

857 Berlin, M. M., & Anderson, R. S. (2007). Modeling of knickpoint retreat on the Roan Plateau, western
858 Colorado. Journal of Geophysical Research: Earth Surface, 112(F3).

859 Bertini, A., Magi, M., Mazza, P. P., & Fauquette, S. (2010). Impact of short-term climatic events on
860 latest Pliocene land settings and communities in Central Italy (Upper Valdarno basin). Quaternary
861 International, 225(1), 92-105.

862 Bertini, T., Bosi, C., (1993). La tettonica quaternaria della conca di Fossa (L'Aquila). Quat.

863 Blumetti, A. M., Di Manna, P., Comerci, V., Guerrieri, L., & Vittori, E. (2017). Paleoseismicity of
864 the san demetrio ne'Vestini fault (L'Aquila basin, Central Italy): implications for seismic
865 hazard. Quaternary International, 451, 129-142.

Blumetti, A.M., Guerrieri, L., Vittori, E., (2013). The primary role of the Paganica-San Demetrio fault system in the seismic landscape of the Middle Aterno Valley basin (Central Apennines). Quat. Int. 288, 183–194. https://doi.org/10.1016/j.quaint.2012.04.040

Bogaart, P. W., & Van Balen, R. T. (2000). Numerical modeling of the response of alluvial rivers to Quaternary climate change. Global and Planetary Change, 27(1-4), 147-163.

Boncio, P., Lavecchia, G., Milana, G., Rozzi, B., 2004a. Seismogenesis in Central Apennines, Italy: An integrated analysis of minor earthquake sequences and structural data in the Amatrice-Campotosto area. Ann. Geophys. 47, 1723–1742. https://doi.org/10.4401/ag-7227

Boncio, P., Lavecchia, G., Pace, B., 2004b. Defining a model of 3D seismogenic sources for Seismic Hazard Assessment applications: The case of central Apennines (Italy). J. Seismol. 8, 407–425. https://doi.org/10.1023/B:JOSE.0000038449.78801.05

Boncio, P., Pizzi, A., Brozzetti, F., Pomposo, G., Lavecchia, G., Di Naccio, D., Ferrarini, F., 2010. Coseismic ground deformation of the 6 April 2009 L'Aquila earthquake (central Italy, M w 6.3). Geophys. Res. Lett. 37, n/a-n/a. https://doi.org/10.1029/2010GL042807

Bosi, C., Galadini, F., Giaccio, B., Messina, P., Sposato, A., 2003. Plio-Quaternary continental deposits in the Latium-Abruzzi Apennines: the correlation of geological events across different intermontane basins. Quat. 16, 55–76.

Bøtter-Jensen, L., E. Bulur, G.A.T. Duller, A.S. Murray (2000). Advances in luminescence instrument systems Radiat. Meas., 32, 523-528.

Bridgland, D., & Westaway, R. (2008). Climatically controlled river terrace staircases: a worldwide Quaternary phenomenon. Geomorphology, 98 (3-4), 285-315.

Bull, W. B. (2008). Tectonic geomorphology of mountains: a new approach to paleoseismology. John Wiley & Sons.

Bull, W. B. (2011). Tectonically active landscapes. John Wiley & Sons.

Carafa, M. M., & Bird, P. (2016). Improving deformation models by discounting transient signals in geodetic data: 2. Geodetic data, stress directions, and long-term strain rates in Italy. Journal of Geophysical Research: Solid Earth, 121(7), 5557-5575.

Carminati, E., Doglioni, C., 2012. Alps vs. Apennines: The paradigm of a tectonically asymmetric Earth. Earth-Science Rev. 112, 67–96. https://doi.org/10.1016/j.earscirev.2012.02.004

Cavinato, G. P., & Celles, P. D. (1999). Extensional basins in the tectonically bimodal central Apennines fold-thrust belt, Italy: response to corner flow above a subducting slab in retrograde motion. Geology, 27(10), 955-958.

Centamore, E., Crescenti, U., Dramis, F., Bigi, S., Fumanti, F., Rusciadelli, G., ... & Petitta, M (2006). Note illustrative della Carta Geologica d'Italia alla scala 1: 50.000, Foglio 359 l'Aquila. Servizio Geologico d'Italia-Apat, 128.

Cesi, C., Di Filippo, M., Di Nezza, M., & Ferri, F. (2010). Caratteri gravimetrici della media Valle del Fiume Aterno. In Gruppo di Lavoro MS-AQ, Geologia e Pericolosità Sismica dell'area Aquilana. Microzonazione Sismica per la ricostruzione dell'area Aquilana.

Chadima, M., Hrouda, F., & Melichar, R. (2006). Magnetic fabric study of the SE Rhenohercynian Zone (Bohemian Massif): Implications for dynamics of the Paleozoic accretionary wedge. Tectonophysics, 418(1-2), 93-109.

Chiarabba, C., Jovane, L., & DiStefano, R. (2005). A new view of Italian seismicity using 20 years of instrumental recordings. Tectonophysics, 395(3-4), 251-268.

Chiaraluce, L. (2012). Unravelling the complexity of Apenninic extensional fault systems: A review of the 2009 L'Aquila earthquake (Central Apennines, Italy). Journal of Structural Geology, 42, 2-18.

Choi, J.H., J.W. Kim, A.S. Murray, D.G. Hong, H.W. Chang, C.S. Cheonga (2009). OSL dating of marine terrace sediments on the southeastern coast of Korea with implications for Quaternary tectonics. Quat. Int., 199 (1–2), 3-14

Chorley, R. J., & Kennedy, B. A. (1971). Physical geography: a systems approach. Prentice Hall.

Cinti, F.R., Pantosti, D., De Martini, P.M., Pucci, S., Civico, R., Pierdominici, S., Cucci, L., Brunori, C.A., Pinzi, S., Patera, A., 2011. Evidence for surface faulting events along the Paganica fault prior to the 6 April 2009 L'Aquila earthquake (central Italy). J. Geophys. Res. Solid Earth 116, 1–21. https://doi.org/10.1029/2010JB007988

Civico, R., Pucci, S., De Martini, P.M., Pantosti, D., 2015. Morphotectonic analysis of the long-term surface expression of the 2009 L'Aquila earthquake fault (Central Italy) using airborne LiDAR data. Tectonophysics 644, 108–121. https://doi.org/10.1016/j.tecto.2014.12.024

Civico, R., Sapia, V., Di Giulio, G., Villani, F., Pucci, S., Baccheschi, P., ... & Pantosti, D. (2017). Geometry and evolution of a fault-controlled Quaternary basin by means of TDEM and single-station ambient vibration surveys: The example of the 2009 L'Aquila earthquake area, central Italy. Journal of Geophysical Research: Solid Earth, 122(3), 2236-2259.

Coltorti, M. A. U. R. O., Consoli, M. A. U. R. I. Z. I. O., Dramis, F. R. A. N. C. E. S. C. O., Gentili, B., & Pambianchi, G. (1991). Evoluzione geomorfologica delle piane alluvionali delle Marche centro-meridionali. Geografia Fisica e Dinamica Quaternaria, 14(1), 87-100.

Cyr, A. J., Granger, D. E., Olivetti, V., & Molin, P. (2010). Quantifying rock uplift rates using channel steepness and cosmogenic nuclide–determined erosion rates: Examples from northern and southern Italy. Lithosphere, 2(3), 188-198.

D'Agostino, N., Jackson, J.A., Dramis, F., Funiciello, R., 2001. Interactions between mantle upwelling, drainage evolution and active normal faulting: An example from the Central Apennines (Italy). Geophys. J. Int. 147, 475–497. https://doi.org/10.1046/j.1365-246X.2001.00539.x

D'Agostino, N., Mantenuto, S., D'Anastasio, E., Giuliani, R., Mattone, M., Calcaterra, S., Gambino, P., Bonci, L., (2011). Evidence for localized active extension in the central Apennines (Italy) from global positioning system observations. Geology 39, 291–294. https://doi.org/10.1130/G31796.1

De Gelder, G., Fernández-Blanco, D., Melnick, D., Duclaux, G., Bell, R. E., Jara-Muñoz, J., ... & Lacassin, R. (2019). Lithospheric flexure and rheology determined by climate cycle markers in the Corinth Rift. Scientific reports, 9(1), 1-12.

Devoti, R., Esposito, A., Pietrantonio, G., Pisani, A. R., & Riguzzi, F. (2011). Evidence of large scale deformation patterns from GPS data in the Italian subduction boundary. Earth and Planetary Science Letters, 311(3-4), 230-241.

Di Biase, R. A., Whipple, K. X., Lamb, M. P., & Heimsath, A. M. (2015). The role of waterfalls and knickzones in controlling the style and pace of landscape adjustment in the western San Gabriel Mountains, California. Bulletin, 127(3-4), 539-559.

Dunai, T. J. (2010). Cosmogenic nuclides: principles, concepts and applications in the earth surface sciences. Cambridge University Press.

Emergeo Working Group. (2009). Rilievi geologici di terreno effettuati nell'area epicentrale della sequenza sismica dell'Aquilano del 6 aprile 2009.

Fifield, L. K., Ophel, T. R., Allan, G. L., Bird, J. R., & Davie, R. F. (1990). Accelerator mass spectrometry at the Australian National University's 14UD accelerator: experience and developments. Nuclear Instruments and Methods in Physics Research Section B: Beam Interactions with Materials and Atoms, 52(3-4), 233-237.

Furlani, S., Cucchi, F., Forti, F., & Rossi, A. (2009). Comparison between coastal and inland Karst limestone lowering rates in the northeastern Adriatic Region (Italy and Croatia). Geomorphology, 104(1-2), 73-81.

Galadini, F., Galli, P., 2000. Active Tectonics in the Central Apennines (Italy) – Input Data for Seismic Hazard Assessment. Nat. Hazards 22, 225–270. https://doi.org/10.1023/A:1008149531980

Galli, P. A., Giaccio, B., Messina, P., Peronace, E., & Zuppi, G. M. (2011). Palaeoseismology of the L'Aquila faults (central Italy, 2009, M w 6.3 earthquake): Implications for active fault linkage. Geophysical Journal International, 187(3), 1119-1134.

Galli, P., Galadini, F., Pantosti, D., 2008. Twenty years of paleoseismology in Italy. Earth-Science Rev. 88, 89–117. https://doi.org/10.1016/j.earscirev.2008.01.001

Galli, P., Giaccio, B., Messina, P., 2010. The 2009 central Italy earthquake seen through 0.5 Myr-long tectonic history of the L'Aquila faults system. Quat. Sci. Rev. 29, 3768–3789. https://doi.org/10.1016/j.quascirev.2010.08.018

Ge.Mi.Na. (1963). Ligniti e torbe dell'Italia continentale. ILTE Ed. Torino IP., 319.

Geurts, A. H., Whittaker, A. C., Gawthorpe, R. L., & Cowie, P. A. (2020). Transient landscape and stratigraphic responses to drainage integration in the actively extending central Italian Apennines. Geomorphology, 353, 107013.

Giaccio, B., Galli, P., Messina, P., Peronace, E., Scardia, G., Sottili, G., Sposato, A., Chiarini, E., Jicha, B., Silvestri, S., 2012. Fault and basin depocentre migration over the last 2 Ma in the L'Aquila

2009 earthquake region, central Italian Apennines. Quat. Sci. Rev. 56, 69–88. https://doi.org/10.1016/j.quascirev.2012.08.016

Giraudi, C. (2005). Middle to Late Holocene glacial variations, periglacial processes and alluvial sedimentation on the higher Apennine massifs (Italy). Quaternary Research, 64(2), 176-184.

Godard, V., Ollivier, V., Bellier, O., Miramont, C., Shabanian, E., Fleury, J., ... & ASTER Team. (2016). Weathering-limited hillslope evolution in carbonate landscapes. Earth and Planetary Science Letters, 446, 10-20.

Angelino, A., Bianchi Fasani, G., Bozzano, F., Colasanto, F., Colombi, A., Di Filippo, M., ... & Verrubbi, V. (2010). Macroarea 8 (Poggio Roio, Colle Roio, Roio Piano, S. Rufina Contrada Cavalli). In Gruppo di Lavoro MS-AQ, Microzonazione Sismica delle macroaree. Microzonazione Sismica per la ricostruzione dell'area Aquilana. Regione Abruzzo-Presidenza del Consiglio dei Ministri, Dipartimento della Protezione Civile, L'Aquila.

Gunnell, Y., Jarman, D., Braucher, R., Calvet, M., Delmas, M., Leanni, L., ... & Keddaouche, K. (2013). The granite tors of Dartmoor, Southwest England: rapid and recent emergence revealed by Late Pleistocene cosmogenic apparent exposure ages. Quaternary Science Reviews, 61, 62-76.

Hancock, G. S., & Anderson, R. S. (2002). Numerical modeling of fluvial strath-terrace formation in response to oscillating climate. Geological Society of America Bulletin, 114(9), 1131-1142.

Harkins, N., Kirby, E., Heimsath, A., Robinson, R., & Reiser, U. (2007). Transient fluvial incision in the headwaters of the Yellow River, northeastern Tibet, China. Journal of Geophysical Research: Earth Surface, 112(F3).

Head,M.J., Gibbard, P.L., 2015. Early-Middle Pleistocene transitions: linking terrestrial and marine realms. Quat. Internat. 389, 7–46.

Heimsath, A. M., Dietrich, W. E., Nishiizumi, K., & Finkel, R. C. (2001). Stochastic processes of soil production and transport: Erosion rates, topographic variation and cosmogenic nuclides in the Oregon Coast Range. Earth Surface Processes and Landforms: The Journal of the British Geomorphological Research Group, 26(5), 531-552.

Herrmann, R. B., Malagnini, L., & Munafò, I. (2011). Regional moment tensors of the 2009 L'Aquila earthquake sequence. Bulletin of the Seismological Society of America, 101(3), 975-993.

Hetzel, R., Niedermann, S., Tao, M., Kubik, P. W., Ivy-Ochs, S., Gao, B., & Strecker, M. R. (2002). Low slip rates and long-term preservation of geomorphic features in Central Asia. Nature, 417(6887), 428-432.

Hippolyte, J. C., Brocard, G., Tardy, M., Nicoud, G., Bourlès, D., Braucher, R., ... & Souffaché, B. (2006). The recent fault scarps of the Western Alps (France): Tectonic surface ruptures or gravitational sackung scarps? A combined mapping, geomorphic, levelling, and 10Be dating approach. Tectonophysics, 418(3-4), 255-276.

Hunstad, I., Selvaggi, G., D'agostino, N., England, P., Clarke, P., & Pierozzi, M. (2003). Geodetic strain in peninsular Italy between 1875 and 2001. Geophysical Research Letters, 30(4).

Improta, L., Villani, F., Bruno, P.P., Castiello, A., Rosa, D. De, Varriale, F., Punzo, M., Brunori, C.A., Civico, R., Pierdominici, S., Berlusconi, A., Giacomuzzi, G., 2012. High-resolution controlled-source seismic tomography across the Middle Aterno basin in the epicentral area of the 2009, Mw 6.3, L'Aquila earthquake (central Apennines, Italy). Ital. J. Geosci. 131, 373–388. https://doi.org/10.3301/IJG.2011.35

ISPRA, ENI (2009). Cartografia Gravimetrica Digitale d'Italia alla scala 1: 250.000.

Kirby, E., Studies, C., Barbara, S., 2001. Quantifying differential rock-uplift rates via stream profile analysis 6, 415–418.

Kirby, E., Whipple, K.X., 2012. Expression of active tectonics in erosional landscapes. J. Struct. Geol. 44, 54–75. https://doi.org/10.1016/j.jsg.2012.07.009

Lavé, J., & Avouac, J. P. (2001). Fluvial incision and tectonic uplift across the Himalayas of central Nepal. Journal of Geophysical Research: Solid Earth, 106(B11), 26561-26591.

Lavecchia, G., Ferrarini, F., Brozzetti, F., De Nardis, R., Boncio, P., & Chiaraluce, L. (2012). From surface geology to aftershock analysis: Constraints on the geometry of the L'Aquila 2009 seismogenic fault system. Italian Journal of Geosciences, 131(3), 330-347.

Lisiecki, L.E., Raymo, M.E., 2005. A Pliocene-Pleistocene stack of 57 globally distributed benthic δ18O records. Paleoceanography 20, 1–17. https://doi.org/10.1029/2004PA001071

Macrì, P., Smedile, A., Speranza, F., Sagnotti, L., Porreca, M., Mochales, T., & Ermolli, E. R. (2016). Analysis of a 150 m sediment core from the co-seismic subsidence depocenter of the 2009 Mw= 6.1 L'Aquila earthquake (Italy): Implications for Holocene-Pleistocene tectonic subsidence rates and for the age of the seismogenic Paganica fault system. Tectonophysics, 687, 180-194.

Merritts, D., & Vincent, K. R. (1989). Geomorphic response of coastal streams to low, intermediate, and high rates of uplift, Medocino triple junction region, northern California. Geological Society of America Bulletin, 101(11), 1373-1388.

Messina, P., Moro, M., & Speranza, F. (2001). Primi risultati di stratigrafia magnetica su alcune formazioni continentali dell'alta valle dell'Aterno (Italia centrale). Il Quaternario, 14, 167-172.

Moro, M., Gori, S., Falcucci, E., Saroli, M., Galadini, F., Salvi, S., 2013. Historical earthquakes and variable kinematic behaviour of the 2009 L'Aquila seismic event (central Italy) causative fault, revealed by paleoseismological investigations. Tectonophysics 583, 131–144. https://doi.org/10.1016/j.tecto.2012.10.036

Murray, A. S., & Wintle, A. G. (2003). The single aliquot regenerative dose protocol: potential for improvements in reliability. Radiation measurements, 37(4-5), 377-381.

Murray, A.S., and Wintle A.G (2000). Luminescence dating of quartz using an improved single-aliquot regenerative-dose protocol, Radiat. Meas., 32 (1), 57-73.

Nesci, O., Savelli, D., & Troiani, F. (2012). Types and development of stream terraces in the Marche Apennines (central Italy): a review and remarks on recent appraisals. Géomorphologie: relief, processus, environnement, 18(2), 215-238.

Nocentini, M., Cosentino, D., Spadi, M., & Tallini, M. (2018). Plio-Quaternary geology of the Paganica-San Demetrio-Castelnuovo Basin (Central Italy). Journal of Maps, 14(2), 411-420.

Olivetti, V., Cyr, A. J., Molin, P., Faccenna, C., & Granger, D. E. (2012). Uplift history of the Sila Massif, southern Italy, deciphered from cosmogenic 10Be erosion rates and river longitudinal profile analysis. Tectonics, 31(3).

Pace, B., Peruzza, L., Lavecchia, G., & Boncio, P. (2006). Layered seismogenic source model and probabilistic seismic-hazard analyses in central Italy. Bulletin of the Seismological Society of America, 96(1), 107-132.

Papanikolaou, I. D., Foumelis, M., Parcharidis, I., Lekkas, E. L., & Fountoulis, I. G. (2010). Deformation pattern of the 6 and 7 April 2009, M W= 6.3 and M W= 5.6 earthquakes in L'Aquila (Central Italy) revealed by ground and space-based observations. Natural Hazards and Earth System Sciences, 10(1), 73-87.

Pazzaglia, F. J. (2003). Landscape evolution models. Developments in Quaternary Sciences, 1, 247-274.

Pazzaglia, F. J., Gardner, T. W., & Merritts, D. J. (1998). Bedrock fluvial incision and longitudinal profile development over geologic time scales determined by fluvial terraces. Geophysical Monograph-American Geophysical Union, 107, 207-236.

Pérez-Peña, J. V., Azañón, J. M., Azor, A., Tuccimei, P., Della Seta, M., & Soligo, M. (2009). Quaternary landscape evolution and erosion rates for an intramontane Neogene basin (Guadix–Baza basin, SE Spain). Geomorphology, 106(3-4), 206-218.

Pérez-Peña, J. V., Azor, A., Azañón, J. M., & Keller, E. A. (2010). Active tectonics in the Sierra Nevada (Betic Cordillera, SE Spain): Insights from geomorphic indexes and drainage pattern analysis. Geomorphology, 119(1-2), 74-87.

Peruzza, L., Pace, B., & Visini, F. (2011). Fault-based earthquake rupture forecast in Central Italy: Remarks after the L'Aquila M w 6.3 event. Bulletin of the Seismological Society of America, 101(1), 404-412.

Phillips, W. M., Hall, A. M., Mottram, R., Fifield, L. K., & Sugden, D. E. (2006). Cosmogenic 10Be and 26Al exposure ages of tors and erratics, Cairngorm Mountains, Scotland: timescales for the development of a classic landscape of selective linear glacial erosion. Geomorphology, 73(3-4), 222-245.

Pizzi, A., Calamita, F. E. R. N. A. N. D. O., Coltorti, M. A. U. R. O., & Pieruccini, P. I. E. R. L. U. I. G. I. (2002). Quaternary normal faults, intramontane basins and seismicity in the Umbria-Marche-Abruzzi Apennine Ridge (Italy): contribution of neotectonic analysis to seismic hazard assessment. Boll. Soc. Geol. It, 1, 923-929.

Pondrelli, S., Salimbeni, S., Morelli, A., Ekstr, G., Olivieri, M., Boschi, E., 2009. earthquake sequence 0, 238–242. https://doi.org/10.1111/j.1365-246X.2009.04418.x

Pondrelli, S., Salimbeni, S., Morelli, A., Ekström, G., Olivieri, M., & Boschi, E. (2010). Seismic moment tensors of the April 2009, L'Aquila (Central Italy), earthquake sequence. Geophysical Journal International, 180(1), 238-242.

Porreca, M., Smedile, A., Speranza, F., Mochales, T., Caracciolo, F. D. A., Di Giulio, G., ... & Sagnotti, L. (2016). Geological reconstruction in the area of maximum co-seismic subsidence during the 2009 Mw= 6.1 L'Aquila earthquake using geophysical and borehole data. Italian Journal of Geosciences, 135(2), 350-362.

Pucci, S., Civico, R., Villani, F., Ricci, T., Delcher, E., Finizola, A., Sapia, V., De Martini, P.M., Pantosti, D., Barde-Cabusson, S., Brothelande, E., Gusset, R., Mezon, C., Orefice, S., Peltier, A., Poret, M., Torres, L., Suski, B., 2016. Deep electrical resistivity tomography along the tectonically active Middle Aterno Valley (2009 L'Aquila earthquake area, central Italy). Geophys. J. Int. 207, 967–982. https://doi.org/10.1093/gji/ggw308

Pucci, S., Mirabella, F., Pazzaglia, F., Barchi, M.R., Melelli, L., Tuccimei, P., Soligo, M., Saccucci, L., 2014. Interaction between regional and local tectonic forcing along a complex Quaternary extensional basin: Upper Tiber Valley, Northern Apennines, Italy. Quat. Sci. Rev. 102, 111–132. https://doi.org/10.1016/j.quascirev.2014.08.009

Pucci, S., Villani, F., Civico, R., Di Naccio, D., Porreca, M., Benedetti, L., ... & Pantosti, D. (2019). Complexity of the 2009 L'Aquila earthquake causative fault system (Abruzzi Apennines, Italy) and effects on the Middle Aterno Quaternary basin arrangement. Quaternary Science Reviews, 213, 30-66.

Pucci, S., Villani, F., Civico, R., Pantosti, D., Del Carlo, P., Smedile, A., De Martini, P.M., Pons-Branchu, E., Gueli, A., 2015. Quaternary geology of the Middle Aterno Valley, 2009 L'Aquila earthquake area (Abruzzi Apennines, Italy). J. Maps 11, 689–697. https://doi.org/10.1080/17445647.2014.927128

Roberts, G. P., Raithatha, B., Sileo, G., Pizzi, A., Pucci, S., Walker, J. F., ... & Walters, R. (2010). Shallow subsurface structure of the 2009 April 6 M w 6.3 L'Aquila earthquake surface rupture at Paganica, investigated with ground-penetrating radar. Geophysical Journal International, 183(2), 774-790.

Roberts, G.P., Michetti, A.M., 2004. Spatial and temporal variations in growth rates along active normal fault systems: An example from The Lazio-Abruzzo Apennines, central Italy. J. Struct. Geol. 26, 339–376. https://doi.org/10.1016/S0191-8141(03)00103-2

Roberts, H.M. (2006). Optical dating of coarse-silt sized quartz from loess: evaluation of equivalent dose determinations and SAR procedural checks- Radiat. Meas., 41 , 923-929.

Rovida, A. N., Locati, M., Camassi, R. D., Lolli, B., & Gasperini, P. (2016). CPTI15, the 2015 version of the Parametric Catalogue of Italian Earthquakes.

Ryb, U., Matmon, A., Erel, Y., Haviv, I., Benedetti, L., Hidy, A.J., 2014. Styles and rates of long-term denudation in carbonate terrains under a Mediterranean to hyper-arid climatic gradient. Earth Planet. Sci. Lett. 406, 142–152. https://doi.org/10.1016/j.epsl.2014.09.008

Santo, A., Ascione, A., Di Crescenzo, G., Miccadei, E., Piacentini, T., & Valente, E., 2014. Tectonic-geomorphological map of the middle Aterno River valley (Abruzzo, Central Italy). J. Maps 10, 365–378. https://doi.org/10.1080/17445647.2013.867545

Saroli, M., Moro, M., Florindo, F., Lancia, M., Lurcock, P.C., & Dinarès-Turell, J., 2015. Paleomagnetic dating of tectonically influenced Plio-Quaternary fan-system deposits from the Apennines (Italy). Ann. Geophys. 58, 1–5. https://doi.org/10.4401/ag-6740

Schimmelpfennig, I., Benedetti, L., Finkel, R., Pik, R., Blard, P.H., Bourlès, D., Burnard, P., Williams, A., 2009. Sources of in-situ 36Cl in basaltic rocks. Implications for calibration of production rates. Quat. Geochronol. 4, 441–461. https://doi.org/10.1016/j.quageo.2009.06.003

Schumm, S. A. (1993). River response to baselevel change: implications for sequence stratigraphy. The Journal of Geology, 101(2), 279-294.

Schwanghart, W., & Scherler, D. (2014). TopoToolbox 2–MATLAB-based software for topographic analysis and modeling in Earth surface sciences. Earth Surface Dynamics, 2(1), 1-7.

Scognamiglio, L., Tinti, E., Michelini, A., Dreger, D.S., Cirella, A., Cocco, M., Mazza, S., Piatanesi, A., 2010. Fast Determination of Moment Tensors and Rupture History: What Has Been Learned from the 6 April 2009 L'Aquila Earthquake Sequence. Seismol. Res. Lett. 81, 892–906. https://doi.org/10.1016/S0169-4332(96)00754-4

Sharma, P., Kubik, P. W., Fehn, U., Gove, H. E., Nishiizumi, K., & Elmore, D. (1990). Development of 36Cl standards for AMS. Nuclear Instruments and Methods in Physics Research Section B: Beam Interactions with Materials and Atoms, 52(3-4), 410-415.

Siame, L., Bellier, O., Braucher, R., Sébrier, M., Cushing, M., Bourlès, D., ... & Yiou, F. (2004). Local erosion rates versus active tectonics: cosmic ray exposure modelling in Provence (south-east France). Earth and Planetary Science Letters, 220(3-4), 345-364.

Snyder, N. P., & Hodges, K. V. (2000). Depositional and tectonic evolution of a supradetachment basin: 40Ar/39Ar geochronology of the Nova Formation, Panamint Range, California. Basin Research, 12(1), 19-30.

Spadi, M., Gliozzi, E., Cosentino, D., & Nocentini, M. (2016). Late Piacenzian–Gelasian freshwater ostracods (Crustacea) from the L'Aquila Basin (central Apennines, Italy). Journal of Systematic Palaeontology, 14(7), 617-642.

Starkel, L. (2003). Climatically controlled terraces in uplifting mountain areas. Quaternary Science Reviews, 22(20), 2189-2198.

Tallini, M., Cavuoto, G., Del Monaco, F., Di Fiore, V., Mancini, M., Caielli, G., ... & Rapolla, A. (2012). Seismic surveys integrated with geological data for in-depth investigation of Mt. Pettino active Fault area (Western L'Aquila Basin). Italian Journal of Geosciences, 131(3), 389-402.

Tarquini, S., Vinci, S., Favalli, M., Doumaz, F., Fornaciai, A., & Nannipieri, L. (2012). Release of a 10-m-resolution DEM for the Italian territory: Comparison with global-coverage DEMs and anaglyph-mode exploration via the web. Computers & geosciences, 38(1), 168-170.

Tucker, G E and Whipple, K.X., 2002. Topographic outcomes predicted by stream erosion models : Sensitivity analysis and intermodel comparison 107, 1–16. https://doi.org/10.1029/2001JB000162

Valoroso, L., Chiaraluce, L., Piccinini, D., Di Stefano, R., Schaff, D., & Waldhauser, F. (2013). Radiography of a normal fault system by 64,000 high-precision earthquake locations: The 2009 L'Aquila (central Italy) case study. Journal of Geophysical Research: Solid Earth, 118(3), 1156-1176.

Vannoli, P., Burrato, P., Fracassi, U., & Valensise, G. (2012). A fresh look at the seismotectonics of the Abruzzi (Central Apennines) following the 6 April 2009 L'Aquila earthquake (Mw 6.3). Italian Journal of Geosciences, 131(3), 309-329.

Villani, F., Improta, L., Pucci, S., Civico, R., Bruno, P.P.G., Pantosti, D., 2017. Investigating the architecture of the Paganica Fault (2009Mw6.1 earthquake, central Italy) by integrating high-resolution multiscale refraction tomography and detailed geological mapping. Geophys. J. Int. 208, 403–423. https://doi.org/10.1093/gji/ggw407

Villani, F., Tulliani, V., Sapia, V., Fierro, E., Civico, R., & Pantosti, D. (2015). Shallow subsurface imaging of the Piano di Pezza active normal fault (central Italy) by high-resolution refraction and electrical resistivity tomography coupled with time-domain electromagnetic data. Geophysical Supplements to the Monthly Notices of the Royal Astronomical Society, 203(3), 1482-1494.

Watchman, A. L., & Twidale, C. R. (2002). Relative and 'absolute'dating of land surfaces. Earth-Science Reviews, 58(1-2), 1-49.

Wegmann, K. W., & Pazzaglia, F. J. (2009). Late Quaternary fluvial terraces of the Romagna and Marche Apennines, Italy: Climatic, lithologic, and tectonic controls on terrace genesis in an active orogen. Quaternary Science Reviews, 28(1-2), 137-165.

Whipple, K.X. &, Tucker, G.E., 1999. Dynamics of the stream-power river incision model: Implications for height limits of mountain ranges, landscape response timescales, and research needs 104, 661–674.

Whittaker, A. C., Attal, M., & Allen, P. A. (2010). Characterising the origin, nature and fate of sediment exported from catchments perturbed by active tectonics. Basin Research, 22(6), 809-828.

Whittaker, A. C., Cowie, P. A., Attal, M., Tucker, G. E., & Roberts, G. P. (2007b). Contrasting transient and steady-state rivers crossing active normal faults: New field observations from the Central Apennines, Italy. Basin Research, 19(4), 529-556.

Whittaker, A.C., Attal, M., Cowie, P.A., Tucker, G.E., Roberts, G., 2008. Decoding temporal and spatial patterns of fault uplift using transient river long profiles. Geomorphology 100, 506–526. https://doi.org/10.1016/j.geomorph.2008.01.018

Whittaker, A.C., Boulton, S.J., 2012. Tectonic and climatic controls on knickpoint retreat rates and landscape response times. J. Geophys. Res. 117, F02024.

Whittaker, A.C., Cowie, P.A., Attal, M., Tucker, G.E., Roberts, G.P., (2007a). Bedrock channel adjustment to tectonic forcing: Implications for predicting river incision rates. Geology 35, 103–106. https://doi.org/10.1130/G23106A.1

Willeit, M., Ganopolski, A., Calov, R., & Brovkin, V. (2019). Mid-Pleistocene transition in glacial cycles explained by declining CO2 and regolith removal. Science Advances, 5(4), eaav7337.

Wobus, C., Whipple, K. X., Kirby, E., Snyder, N., Johnson, J., Spyropolou, K., ... & Willett, S. D. (2006). Tectonics from topography: Procedures, promise, and pitfalls. Special papers-geological Society of America, 398, 55.

Zhang, J. Y., Liu-Zeng, J., Scherler, D., Yin, A., Wang, W., Tang, M. Y., & Li, Z. F. (2018). Spatiotemporal variation of late Quaternary river incision rates in southeast Tibet, constrained by dating fluvial terraces. Lithosphere, 10(5), 662-675.

Zhou, M., Xia, J., Lu, J., Deng, S., & Lin, F. (2017). Morphological adjustments in a meandering reach of the middle Yangtze River caused by severe human activities. Geomorphology, 285, 325-332.